SKB

TECHNICAL REPORT 89-08

NAK WP-Cave Project
Thermally induced convective motion in groundwater in the near field of the WP-Cave after filling and closure

Robert J. Hopkirk

Polydynamics Ltd., Zürich, Switzerland

April 1989

SVENSK KÄRNBRÄNSLEHANTERING AB
SWEDISH NUCLEAR FUEL AND WASTE MANAGEMENT CO

BOX 5864 S-102 48 STOCKHOLM

TEL 08-665 28 00 TELEX 13108 SKB S
TELEFAX 08-661 57 19

NAK WP-CAVE PROJECT
THERMALLY INDUCED CONVECTIVE MOTION IN GROUNDWATER IN THE NEAR FIELD OF THE WP-CAVE AFTER FILLING AND CLOSURE

Robert J. Hopkirk

Polydynamics Ltd., Zürich, Switzerland

April 1989

SKB WP-CAVE PROJECT

Thermally induced convective motion in groundwater in the near field of the WP-Cave after filling and closure

Robert J. Hopkirk
Polydynamics Ltd., Zürich, Switzerland

April 1989

Abstract

The thermal convective motion induced in groundwater due to the decay heat generated by the high level waste in the WP-Cave has been studied by means of coupled thermo-hydraulic numerical models. The WPC concept is proposed as an alternative to the KBS-3 repository concept for construction in crystalline rock. However, in the absence of specific site fissure data, the rock mass has been modelled as a quasi-porous medium.

The repository was assumed to be filled 40 years after unloading of the fuel from its reactors. For a further 100 years the whole repository is cooled, before being backfilled and sealed off. Maximum waste temperatures and the fluid fluxes crossing the backfilled bentonite diffusion barrier were monitored to 3000 years after fuel unloading. At the same time, the effects of the hydraulic cage and of a highly permeable rock zone beneath the central storage volume on the induced fluid flows have been assessed.

Keywords

Buoyancy, High level waste, Hydraulic cage, Numerical model, Thermal convection, Thermo-hydraulic coupling, Residual heat generation, Waste temperature, WP-Cave.

List of Contents

Summary

The compact design of the WP-Cave concept leads to concern for high waste temperatures. In addition, the buoyancy forces in a continuous, saturated rock mass can be expected to induce convective cell motion in the pore and fissure water in the surrounding host rock.

In order to assess the orders of magnitude of the temperature field and of the strength of the induced flows, a numerical modelling programme has been pursued. To this end a model was set up in cylindrical coordinates with the finite difference flow and transport code TROF-2DP, thereby making use of the economies offered by the WP-Cave geometry. The materials were represented as quasi-porous media since no specific site (with its associated fissure data) was under consideration.

Initial heat loads of 1.13, 0.81 and 0.6MW at the time of waste placement in the repository were considered. The essential circumferential "smearing" of the storage channels, a consequence of the cylindrical model, has resulted in estimates of peak temperatures which are slightly higher than in the detailed near-field thermal calculations (see SKB TR 89-26), so that the lowest heat loading of 0.6MW yielded a maximum temperature in the centre of the storage region of 160°C rather than 150°C.

The study reveals that the density of the bentonite/sand diffusion barrier plays a significant rôle in reducing the amount of water flowing upwards through the storage volume in the primary convection cell.

The hydraulic cage, the outermost constructive element in the WPC concept, reduces the flow of groundwater through the storage region but has a very minor effect upon the thermally driven convective flows originating within it. If solute does cross the bentonite/sand barrier, the presence of the cage and the modifications it causes to the outer portions of the convective motion will tend to mix the solutes with that groundwater carried by the cage. The existence of this mechanism accentuates the importance of the quality of the bentonite/sand barrier.

A hypothetical, highly permeable zone was introduced in the host rock, crossing the model domain horizontally immediately below the storage region. Its presence does not radically increase the flow through the repository, but stimulates the motion between the bentonite barrier and the hydraulic cage and hence the mixing within this outer region of any solutes which do escape across the diffusion barrier. This result underlines the need for site qualification.

1. Introductory Remarks

The WP-Cave concept for the storage and final disposal of high level radioactive wastes involves the hydraulic isolation of an essentially cylindrical storage volume from passing groundwater by means of a two- stage barrier.

The first (inner) stage is a diffusive barrier formed by a 5 m thick enclosure of backfilled bentonite in an excavated annular space surrounding the storage volume. The second stage is a hydraulic "cage" formed by a network of drillholes and ring galleries. Figure 1 is a reproduction of this overall geometry.

The purpose of the present report is to present the results of preliminary calculations of coupled thermo-hydraulic processes in the near field. These have been undertaken to check whether thermally induced circulations within either of the two barriers could diminish the effectiveness of the barriers themselves.

The work has been carried through in two stages. In the first stage a uniform distribution of the heat source intensity within the storage region was assumed. A more detailed model of the heat source was introduced in the second stage calculations. In both stages, the WP-Cave was modelled with and without the presence of the hydraulic cage. The following parameters have been varied:

- the magnitude of the heat source
- hydraulic conductivity of the bentonite barrier
- hydraulic conductivity of the inner rock mass

2. The Model

2.1 General overview - geometric representation

A mathematical model of the near field of the WP-Cave has been constructed using the cylindrical coordinate feature of the hydrological transport code TROUGH-2DP, [1], whereby advantage has been taken of the cylindrical nature of the WP-Cave geometry in order to be able to make use of this feature and to avoid the necessity of creating a three dimensional model. The resulting model domain may be thought of as a "cake slice". The idealised geometry is illustrated in Figure 2. In this figure, the vertical axis (z) coincides with the vertical axis of symmetry of the WP-Cave.

Figure 3 shows the simplified geometry finally adopted for economy of modelling. The combination of buoyancy source terms in the hydraulic equation for every discrete volume over the field and the extreme contrasts of thermal conductivity between the cage and the neighbouring host rock (10^5 compared with 10^{-9} ms-1) have demanded fine discretisation of the problem in both space and time.

The conical features of the bentonite barrier and of the hydraulic cage have been replaced by horizontal discs to enable the number of discrete volumes and hence the time of computation to be reduced. This reflects the constraint imposed by the finite differencing in the TROUGH code to the use of rectangular control volumes. The orders of magnitude of the hydraulic flow vectors leaving the bentonite barrier are maintained in spite of the simplification.

The first stage model consisted of 29 (radial direction) by 38 (vertical) nodes. This was verified successfully for the situation without the hydraulic cage against a more refined model (31 by 70 nodes), which included the conical features of the bentonite barrier. The model size necessary for a satisfactory representation of the conical portions of the hydraulic cage to the same level of detail was 112 by 150 nodes. Since the results sought from the model were principally the fluxes across the bentonite barrier, the simplified representation of the cage geometry was judged to be worthwhile and justifiable.

The second stage model contains more detail in the heat generating storage volume than the two versions discussed above, but the conical features remain absent. The model dimensions were 34 by 75 nodes.

One consequence of the use of cylindrical geometry is the implicit acceptance of axi-symmetry not only of construction and of material properties, but also of physical processes. Thus, no transversal groundwater flow has been considered and the only source of fluid flow is buoyancy forces.

2.2 Assumptions in the model

The physical system:

There are three basically different ways in which diffusive/ advective heat transport in a fluid-filled permeable medium can be simulated:

- to assume that the fluid is always locally at the same temperature as the solid matrix material;
- to assume that the solid material locally has a characteristic temperature which the fluid does not attain in real times because of the action of a heat transfer resistance between the two media;
- to assume that the solid is composed of blocks of material so large that heat exchange with a passing fluid at their surfaces influences the temperature distribution within each particular block. The fluid may then be assumed either to take the surface temperature of the solid locally or to exchange heat with the solid surface via a heat transfer resistance.

In the present case the first and simplest model has been used in order to establish primarily the expected orders of magnitude of the coupled effects.

This model assumption may be applied to situations in which very slow fluid flows occur even when the grain or block size of the solid is substantial. As will be seen later, the slow flow assumption appears to be justified in the present case. So far, although the necessary algorithm is available, no check has been made on the applicability of the implicit assumption in this model of locally uniform temperature distributions across grains or blocks.

The result of selecting the first of the three alternative model assumptions is that the repository host material is forced to correspond to a porous medium. The equations for coupled heat and fluid transport in such a material are presented in Appendices I and II.

Thermal-hydraulic coupling:

Two equations have to be solved at each step in time, one for fluid flow and one for thermal energy transport. The first is a diffusion equation, if the Darcy flow assumption is maintained; the second a standard advection diffusion transport equation.

Buoyancy forces are reflected by the inclusion in the head diffusion equation of potential sources, which perturb the potential field and thus modify the fluid flows. The flow field is accounted for in the thermal energy transport equation by the advective transport terms, which contain the velocity components in the orthogonal coordinate directions.

If the fluid fluxes are sufficiently small in this induced flow field the contribution of advective transport becomes insignificant. In the present case, the low flow porosities and permeabilities create such a situation, so the further simplification of only partial coupling could be permitted in the final calculations. Partial coupling permits the buoyancy forces to affect the flow field, but the advective transport terms in the thermal energy equation may be dropped. Such a step saves several global iterations of the field solutions in each timestep, thus reducing computational time by a factor of at least three (three global iterations is the minimum allowed in the TROUGH code for fully coupled solutions). The assumption of partial coupling was therefore adapted.

The Waste and the Excavations - Initial Conditions:

A further assumption made in the model concerns the intensity of heat generation. For these rather preliminary calculations it has been (conservatively) assumed that the entire waste inventory is deposited simultaneously in the storage cavern forty years after unloading from the reactors.

For a period of one hundred years after the placement of the used fuel the repository is cooled forcibly so that the cooling air does not exceed 40°C. At this time (140 years from unloading) the repository is closed.

Simultaneously with the closure, the whole gallery/shaft system is assumed to be rapidly backfilled with a sand/water mixture and the surrounding rock mass, which will in reality have been drained of water, is furthermore assumed to become instantly resaturated. Thereafter, long-term effects on the hydraulic system, caused by convergence of the excavations are ignored.

3. Heat Source Initial and Boundary Conditions

3.1 The Heat Source Intensity

Figure 4 shows the specific heat release rate time history for PWR spent fuel after a burn up to 38'000 MWd/ton Uranium. These data have been published in SKN Report 16 [4]. This curve has been approximated by a fifth order polynomial in ($\log_{10}t$):

$$\dot{Q}(t) = Q_0 \cdot 10^{\left(\sum_{m=0}^{5} a_m [\log_{10} t]^m\right)} \qquad (3.1)$$

The resulting curve of this polynomial function, derived by a least squares error fitting procedure is also plotted on Figure 4. The maximum discrepancy between the data curve and the fitted curve is of the order of 3% at ca. 200 years after unloading. Table 3-1 below lists the coefficients a_m:

Coefficient	Value
a_0	4.041038×10^{0}
a_1	-6.134463×10^{-1}
a_2	-9.398288×10^{-1}
a_3	9.499749×10^{-1}
a_4	-3.287113×10^{-1}
a_5	3.707720×10^{-2}

Table 3-1: Coefficients of the logarithmic polynomial heat source function.

As stated above, the entire inventory is assumed to be placed in the repository simultaneously, 40 years after unloading from reactor. At this instant, the start of the model calculation, three levels of heat output have been used: 1.13 MW, 0.81 MW and 0.60 MW. In each case, Q_0 has been normalised to the desired level. During the first 100 years following disposal a thermal sink is applied to the model volume representing the waste caverns to maintain the temperature at the desired temperature of 40°C. The strength of the volumetric heat source intensity, S_T, is obtained by scaling Q_0 to account for the relation between the real waste package and model source domain volumes.

3.2 Initial and Boundary Conditions

General:

Apart from the upper boundary, which represents the upper limit of the groundwater system and is at a predetermined height above the repository, the other boundaries are selected to provide sufficient buffer volume between themselves and the perturbation represented by the heat-generating waste. This becomes apparent upon studying Figures 2 and 3.

Hydraulic:

The upper and lower horizontal boundaries have been fixed as no-flow (zero head gradient) boundaries whilst the outer radial boundary is fixed at the initial head level for the whole field of 10.0 m.
In order to improve the validity of the uniform fixed head value along the vertical, cylindrical outer boundary the outermost cells in the horizontal direction were arbitrarily allotted hydraulic conductivities (K) equal to 10% of that of the host rock. Likewise the storativity coefficients (see Appendix II) were set ten times higher than those host rock. This tactic effectively increases the outer radius of the domain. The last 300 m are thereby effectively to 3 km.

Thermal:

The seabed temperature in the case of coastal sub-seabed disposal is defined at 4°C and the typical vertical geothermal gradient, corresponding to a radial earth heat flux of 50 mW/m^2 varies little from 1.4°C per 100 m over the first 1000 m of depth below the surface. These geothermal values imply that all significant geothermal heat flow must be via conduction. In its turn this statement implies that advective vertical heat transport is negligible. Thus the vertical connectivity of the hydraulic system is weak. A continuously connected system with no apparent resultant water inflows or outflows at the surface would tend to experience large scale free convection circulations of fluid throughout its whole volume, resulting in a somewhat reduced geothermal gradient. Distinct upwards or downwards regional water movement over long periods arising with the formation of convection cells will cause characteristic distortion of the temperature gradient resulting from pure conduction alone.

For conservatism in the present case, which concerns a generic site, a continuously connected active hydraulic system has been assumed. An average initial temperature of 9.6°C was employed for the whole domain, corresponding to the initial true temperature at the mid-depth of the cave. This temperature level was then also used as the reference temperature for viscosity and density.

The outer boundaries of the domain are maintained fixed at this same temperature during the problem time.

4. Cases Calculated

Three different assumptions regarding the design have been considered:

- no hydraulic cage

- with hydraulic cage

- with hydraulic cage, but in addition a 10 m wide horizontal, highly permeable (2×10^{-6} ms^{-1}) band directly below the repository storage volume.

In addition, the thermal load of the radioactive waste and the hydraulic properties of the near field materials were varied for the different cases calculated. Table 4-1 gives an overview of all the cases calculated. All relevant parameters and material properties are described in Chapter 5. It should be noted that for the last set of these calculations (Cases 6 to 8), a set of conservative hydraulic parameters were used in the region within the bentonite diffusion barrier. The conductivity of the bentonite shell itself was raised by one order of magnitude and the conductivity of the rock within the barrier was raised by two orders of magnitude. The intention here was to make allowance for decompression and additional cracking in the rock following the excavation of the surrounding shell.

Table 4-1: Cases Calculated

First Stage

Case No.	No hydraulic cage Uniform host rock	With hydraulic cage Uniform host rock	Permeable rock zone below storage volume	Heat load [MW]	Material Variations
A	x			1.13	
B		x		1.13	
C			x	1.13	

Second Stage

1	x			0.81	Model refinements introduced. Hydraulic conductivity raised in upper part of bentonite shell and reduced in lower part
2		x		0.81	
3			x	0.81	
4	x			1.13	
5	x			0.81	Reduced hydraulic conductivity in upper half of bentonite shell also
6	x			0.6	Uniformly raised hydraulic conductivity of bentonite shell and enhanced hydraulic conductivity of the (decompressed) rock mass within the bentonite shell (conservative material set)
7		x		0.6	
8			x	0.6	

5. Thermal Load and Material Properties

For the initial (first stage) calculations the thermal load of the waste was set to 1.13 MW, the value corresponding to the full tonnage load of the WP-Cave repository. However a maximum allowable temperature criterion of 150°C was introduced in the course of the safety analysis. This was achieved by decreasing the tonnage of spent fuel in the repository to a level corresponding to an initial thermal loading of 0.81 MW. Since the geometrically simplified source model used in the present study tends to overestimate the peak temperatures, it was decided to reduce the thermal loading still further, rather than develop a more accurate near field model. Therefore an initial thermal loading of 0.6 MW was applied to the last calculations. The initial thermal load strength is tabulated against the maximum temperature in Table 5-1 below.

Table 5-1: Thermal Source Term and Resulting Peak Temperatures According to here Used Simplified Temperature Calculation Model.

Case No.	Thermal Load Inserted 40 yrs old fuel [MW]	Peak Temperatures, approx figures [°C]
A-C	1.13	280
1-3	0.81	205
4	1.13	275
5	0.81	205
6-8	0.6	160

The Tables 5-2, 5-3 and 5-4 present all essential properties of solid material used for the calculations. It will be noticed that in Tables 5-2 and 5-3 the hydraulic conductivity of the host rock is given as a continuous function of depth. A stepwise variation of this property has finally been used in the model.

Table 5-5 contains the properties of the groundwater with exception of the viscosity. This is calculated as an exponential function as given below:

$$\ln \mu = \sum_{m=1}^{4} b_m T^m \qquad 5.1$$

The coefficients in this expansion for viscosity of pure water are listed in Table 5-6. They are derived from data in Schmidt & Grigull [5].

Table 5-2: Material Properties of the undisturbed Host Rock

Hydraulic Conductivity [ms^{-1}]	$2.17 \times 10^{-6} \times d^{-1.08}$ (d is depth [m])
Flow Porosity [-]	1.0×10^{-4}
Density of Solid Fraction [kgm^{-3}]	2.7×10^{3}
Volumetric Modulus of Compressibility of Solid Part [Pa^{-1}]	9.0×10^{-11}
Thermal Conductivity of Saturated Solid [$Wm^{-1}K^{-1}$]	$3.6 - 3.74 \times 10^{-3}$ T [T in °C]
Cubical Expansion Coefficient [K^{-1}]	1.8×10^{-5}
Specific Heat of Solid Fraction [$JKg^{-1}K^{-1}$]	8.0×10^{2}

Table 5-3: Material Properties used for Regions Inside the Bentonite/Sand Barrier

Hydraulic Conductivity [ms^{-1}]	Cases A-C	Cases 1-5	Cases 6-8
Whole Volume (A-C); Rock surrounding Waste (1-8)	$2.17x10^{-6}d^{-1.08}$	$2.0x10^{-9}$	$2.0x10^{-7}$
Sand/Water Backfill (Central Shaft)	-	$1.0x10^{-5}$	
Storage Volume (Host Rock, Channels, Waste)	-	h: $4.0x10^{-7}$ v: $1.0x10^{-9}$	h: $2.5x10^{-6}$ v: $9.0x10^{-7}$
Flow Porosity [-]	Cases A-C	Cases 1-5	Cases 6-8
Whole Volume (A-C); Rock surrounding Waste (1-8)	$1.0x10^{-4}$	$1.0x10^{-3}$	
Sand/Water Backfill (Central Shaft)	-	$1.0x10^{-2}$	$1.0x10^{-3}$
Storage Volume (Host Rock, Channels, Waste)	-	$1.0x10^{-2}$	$1.0x10^{-3}$
Density of Solid Fraction [kgm^{-3}]	Cases A-C	Cases 1-5	Cases 6-8
Whole Volume (A-C); Rock surrounding Waste (1-8)	$2.7x10^{3}$		
Sand/Water Backfill (Central Shaft)	-	$2.2x10^{3}$	
Storage Volume (Host Rock, Channels, Waste)	-	$2.8x10^{3}$	
Thermal Conductivity of Saturated Solid [$Wm^{-1}K^{-1}$]	Cases A-C	Cases 1-5	Cases 6-8
Whole Volume (A-C); Rock surrounding Waste (1-8)	$3.6 - 3.74x10^{-3}$ T		
Sand/Water Backfill (Central Shaft)	-	2.1	
Storage Volume (Host Rock, Channels, Waste)	-	16.7	
Specific Heat of Solid Fraction [$JKg^{-1}K^{-1}$]	Cases A-C	Cases 1-5	Cases 6-8
Whole Volume (A-C); Rock surrounding Waste (1-8)	$8.0x10^{2}$		
Sand/Water Backfill (Central Shaft)	-	$1.2x10^{3}$	
Storage Volume (Host Rock, Channels, Waste)	-	$7.6x10^{2}$	
Cubical Expansion Coefficient [K^{-1}]	Cases A-C	Cases 1-5	Cases 6-8
Whole Volume (A-C); Rock surrounding Waste (1-8)	$1.8x10^{-5}$		
Sand/Water Backfill (Central Shaft)	-	$3.0x10^{-5}$	
Storage Volume (Host Rock, Channels, Waste)	-	$2.2x10^{-5}$	
Volumetric Modulus of Compressibility of Solid Components [Pa^{-1}]	Cases A-C	Cases 1-5	Cases 6-8
Whole Volume (A-C); Rock surrounding Waste (1-8)	$9.0x10^{-11}$		
Sand/Water Backfill (Central Shaft)	-	$1.0x10^{-9}$	
Storage Volume (Host Rock, Channels, Waste)	-	$9.0x10^{-11}$	

Table 5-4: Material Properties Used for Different Parts of the Bentonite/Sand Barrier

Hydraulic Conductivity [ms^{-1}]	Cases A-C	Cases 1-4	Case 5	Cases 6-8
Upper cone (A-C); upper half (1-8)	$1.0x10^{-11}$	$1.0x10^{-10}$	$1.0x10^{-11}$	$1.0x10^{-10}$
Cylindrical portion	$1.0x10^{-10}$	-	-	-
Lower cone (A-C); lower half (1-8)	$1.0x10^{-10}$	$1.0x10^{-11}$	$1.0x10^{-11}$	$1.0x10^{-10}$

Flow Porosity [-]	Cases A-C	Cases 1-5	Cases 6-8
Upper cone (A-C); upper half (1-8)	$3.3x10^{-1}$	$1.0x10^{-1}$	$5.0x10^{-1}$
Cylindrical portion	$2.5x10^{-1}$	-	-
Lower cone (A-C); lower half (1-8)	$3.0x10^{-1}$	$2.5x10^{-1}$	$2.5x10^{-1}$

Thermal Conductivity [Wm-1K-1]	Cases A-C	Cases 1-8
Upper cone (A-C); upper half (1-8)	2.1	2.1
Cylindrical portion	2.0	-
Lower cone (A-C); lower half (1-8)	3.5	3.5

Cubical Expansion Coefficient [K^{-1}]	All Cases
All zones	$2.5x10^{-5}$
Volumetric Modulus of Compressibility [Pa^{-1}]	All Cases
All zones	$1.0x10^{-11}$ (estimated)
Specific Heat of Solid Fraction [$Jkg^{-1}K^{-1}$]	All Cases
All zones	$8.0x10^{2}$

Table 5-5: Properties of Water

Variable	Value
Reference density [kg m^{-3}]	9.98×10^{2}
Thermal conductivity [W m^{-1} K^{-1}]	0.6
Cubical expansion coefficient [K^{-1}]	1.8×10^{-3}
Compressibility $\beta = 1 / K$ [Pa^{-1}]	4.88×10^{-10}
Specific Heat [J Kg^{-1} K^{-1}]	4.18×10^{3}

Table 5-6: Coefficients for the fitted polynomial exponent of the expression for viscosity (5.1)

Coefficient	Value
b_1	$-2.9095017 \times 10^{-2}$
b_2	1.4100172×10^{-4}
b_3	$-3.6361410 \times 10^{-7}$
b_4	$3.4843856 \times 10^{-10}$

6. PRESENTATION OF RESULTS

The results of the calculation runs, insofar as they affect transport of solutes from the repository, are exposed in Tables 6-1 to 6-7 for the stage 1 calculations and in Tables 6-8 to 6-12 for the stage 2 calculations. Each table contains a number of reference velocity components at eight (stage 1 calculations) and ten (stage 2 calculations) respectively preselected monitoring points on the outer surface of the bentonite barrier for each of the cases at one particular instant in time. The nodal points of the finite difference cells, whose vector components have been tabulated, are indicated in Figures 5a (stage 1) and 5b (stage 2). The vertical components in monitor cells 1, 2, 7 and 8 in Figure 5a and 1, 2, 3, 8, 9, and 10 in Figure 5b are defined on the outer surface of the bentonite barrier as are the horizontal components in cells 3, 4, 5 and 6 in Figure 5a and 4, 5, 6, and 7 in Figure 5b.

This approach permits the release rates from the near field of the repository, defined here as that volume lying within the bentonite shell, to be determined for input to a migration computation. The monitoring points numbered 1 to 8 (stage 1) and 1 to 10 (stage 2), their coordinates and nodal addresses are shown in Figures 5a and 5b.

Figure 6 shows the resulting temperature in the source region for the two stages and different thermal loads applied. As is seen in the Figure the difference is negligible between the results of Stage 1 and Stage 2 models.

The induced flow, Darcy' s velocity, is presented in Figures 7 to 17. Point 2 in Stage 1 and Point 3 in Stage 2 respectively were selected for the reference vectors. The Figures contain the time histories, up to 3000 years, of both horizontal and vertical velocity components at the reference points, Figure 7 in Case A, Figure 8 for Case B etc.

The general forms of the velocity time histories correlate closely to those of the temperature in the centre of the waste storage region. The storage region heats up very rapidly after the 100 years of controlled cooling following disposal (at t = 40 years), giving rise to a plateau on each curve up to t = 140 years followed by an immediate rise and a slow decay.

Table 6-1: Exit speeds (Darcy velocities in m/yr) out of Bentonite Barrier

		Case A (no cage)	Case B (with cage)	Case C (with cage + h.c. zone)
Time [yrs]		93.6	93.6	93.6
Max Temperatures [°C]				
Sources	(3/21)	$4.00 \times 10^{+1}$	$4.00 \times 10^{+1}$	$4.00 \times 10^{+1}$
Cage	(16/21)	$1.24 \times 10^{+1}$	$1.20 \times 10^{+1}$	$1.20 \times 10^{+1}$
U1	(4/26)	1.09×10^{-6}	6.09×10^{-7}	3.20×10^{-6}
W1		3.81×10^{-5}	3.50×10^{-5}	1.47×10^{-4}
U2	(8/26)	7.29×10^{-6}	4.02×10^{-6}	2.54×10^{-5}
W2		2.45×10^{-5}	2.15×10^{-5}	1.23×10^{-4}
U3	(10/24)	5.44×10^{-6}	5.06×10^{-6}	1.06×10^{-4}
W3		2.94×10^{-5}	2.01×10^{-5}	4.32×10^{-5}
U4	(10/22)	3.82×10^{-6}	3.66×10^{-6}	1.20×10^{-4}
W4		4.02×10^{-5}	3.06×10^{-5}	6.60×10^{-5}
U5	(10/19)	-3.92×10^{-6}	-3.77×10^{-6}	1.54×10^{-4}
W5		3.38×10^{-5}	2.44×10^{-5}	3.20×10^{-4}
U6	(10/16)	-5.93×10^{-6}	-5.54×10^{-6}	-2.95×10^{-4}
W6		1.66×10^{-5}	1.05×10^{-5}	9.79×10^{-4}
U7	(8/14)	-6.90×10^{-6}	-3.68×10^{-6}	-5.09×10^{-5}
W7		1.03×10^{-5}	1.33×10^{-5}	2.48×10^{-4}
U8	(4/14)	-1.02×10^{-6}	-7.36×10^{-7}	-7.78×10^{-6}
W8		1.41×10^{-5}	2.13×10^{-5}	2.98×10^{-4}

Table 6-2: Exit speeds (Darcy velocities in m/yr) out of Bentonite Barrier

		Case A (no cage)	Case B (with cage)	Case C (with cage + h.c. zone)
Time [yrs]		394	394	394
Max Temperatures [°C]				
Sources	(3/21)	$1.98 \times 10^{+2}$	$1.96 \times 10^{+2}$	$1.96 \times 10^{+2}$
Cage	(16/21)	$4.71 \times 10^{+1}$	$4.70 \times 10^{+1}$	$4.70 \times 10^{+1}$
U1	(4/26)	7.90×10^{-6}	2.33×10^{-6}	1.75×10^{-5}
W1		3.39×10^{-4}	3.25×10^{-4}	1.08×10^{-3}
U2	(8/26)	5.60×10^{-5}	1.04×10^{-5}	1.45×10^{-4}
W2		2.65×10^{-4}	2.50×10^{-4}	9.45×10^{-4}
U3	(10/24)	2.62×10^{-5}	1.57×10^{-5}	6.66×10^{-4}
W3		2.95×10^{-4}	1.42×10^{-4}	3.26×10^{-4}
U4	(10/22)	1.86×10^{-5}	1.34×10^{-5}	7.67×10^{-4}
W4		3.57×10^{-4}	1.92×10^{-4}	5.21×10^{-4}
U5	(10/19)	-1.99×10^{-5}	-1.48×10^{-5}	9.94×10^{-4}
W5		3.16×10^{-4}	1.60×10^{-4}	3.32×10^{-3}
U6	(10/16)	-2.89×10^{-5}	-1.79×10^{-5}	-1.81×10^{-3}
W6		2.02×10^{-4}	1.09×10^{-4}	1.11×10^{-2}
U7	(8/14)	-5.24×10^{-5}	-7.81×10^{-6}	-1.21×10^{-4}
W7		1.41×10^{-4}	2.34×10^{-4}	2.54×10^{-3}
U8	(4/14)	-7.31×10^{-6}	-8.14×10^{-6}	-2.85×10^{-5}
W8		1.69×10^{-4}	2.88×10^{-4}	2.71×10^{-3}

Table 6-3: Exit speeds (Darcy velocities in m/yr) out of Bentonite Barrier

		Case A (no cage)	Case B (with cage)	Case C (with cage + h.c. zone)
Time [yrs]		754	754	754
Max Temperatures [°C]				
Sources	(3/21)	$1.18 \times 10^{+2}$	$1.18 \times 10^{+2}$	$1.18 \times 10^{+2}$
Cage	(16/21)	$3.73 \times 10^{+1}$	$3.72 \times 10^{+1}$	$3.72 \times 10^{+1}$
U1	(4/26)	5.19×10^{-6}	$0.00 \times 10^{+0}$	9.11×10^{-6}
W1		2.42×10^{-4}	2.31×10^{-4}	7.14×10^{-4}
U2	(8/26)	3.76×10^{-5}	-2.60×10^{-6}	7.82×10^{-5}
W2		1.99×10^{-4}	1.88×10^{-4}	6.32×10^{-4}
U3	(10/24)	1.29×10^{-5}	4.83×10^{-6}	4.09×10^{-4}
W3		2.02×10^{-4}	8.38×10^{-5}	2.04×10^{-4}
U4	(10/22)	9.45×10^{-6}	5.49×10^{-6}	4.75×10^{-4}
W4		2.35×10^{-4}	1.09×10^{-4}	3.31×10^{-4}
U5	(10/19)	-1.01×10^{-5}	-6.29×10^{-6}	6.20×10^{-4}
W5		2.14×10^{-4}	9.32×10^{-5}	2.27×10^{-3}
U6	(10/16)	-1.43×10^{-5}	-5.88×10^{-6}	-1.11×10^{-3}
W6		1.51×10^{-4}	8.21×10^{-5}	7.84×10^{-3}
U7	(8/14)	-3.42×10^{-5}	3.91×10^{-6}	-2.72×10^{-5}
W7		1.16×10^{-4}	2.06×10^{-4}	1.81×10^{-3}
U8	(4/14)	-4.69×10^{-6}	-5.81×10^{-6}	-1.44×10^{-5}
W8		1.34×10^{-4}	2.34×10^{-4}	1.88×10^{-3}

Table 6-4: Exit speeds (Darcy velocities in m/yr) out of Bentonite Barrier

		Case A (no cage)	Case B (with cage)	Case C (with cage + h.c. zone)
Time [yrs]		1290	1290	1290
Max Temperatures [°C]				
Sources	(3/21)	$7.16 \times 10^{+1}$	$7.14 \times 10^{+1}$	$7.14 \times 10^{+1}$
Cage	(16/21)	$2.70 \times 10^{+1}$	$2.69 \times 10^{+1}$	$2.69 \times 10^{+1}$
U1	(4/26)	3.21×10^{-6}	-5.81×10^{-7}	5.31×10^{-6}
W1		1.49×10^{-4}	1.43×10^{-4}	4.28×10^{-4}
U2	(8/26)	2.36×10^{-5}	-4.12×10^{-6}	4.25×10^{-5}
W2		1.25×10^{-4}	1.19×10^{-4}	3.82×10^{-4}
U3	(10/24)	6.39×10^{-6}	1.51×10^{-6}	2.38×10^{-4}
W3		1.17×10^{-4}	4.67×10^{-5}	1.18×10^{-4}
U4	(10/22)	4.90×10^{-6}	2.47×10^{-6}	2.77×10^{-4}
W4		1.36×10^{-4}	5.98×10^{-5}	1.94×10^{-4}
U5	(10/19)	-5.33×10^{-6}	-3.04×10^{-6}	3.63×10^{-4}
W5		1.25×10^{-4}	5.16×10^{-5}	1.37×10^{-3}
U6	(10/16)	-7.22×10^{-6}	-2.16×10^{-6}	-6.43×10^{-4}
W6		9.10×10^{-5}	5.03×10^{-5}	4.82×10^{-3}
U7	(8/14)	-2.06×10^{-5}	4.56×10^{-6}	-4.53×10^{-6}
W7		7.39×10^{-5}	1.37×10^{-4}	1.12×10^{-3}
U8	(4/14)	-2.79×10^{-6}	-3.78×10^{-6}	-7.97×10^{-6}
W8		8.42×10^{-5}	1.50×10^{-4}	1.15×10^{-3}

Table 6-5: Exit speeds (Darcy velocities in m/yr) out of Bentonite Barrier

		Case A (no cage)	Case B (with cage)	Case C (with cage + h.c. zone)
Time [yrs]		1470	1470	1470
Max Temperatures [°C]				
Sources	(3/21)	$6.35 \times 10^{+1}$	$6.34 \times 10^{+1}$	$6.34 \times 10^{+1}$
Cage	(16/21)	$2.49 \times 10^{+1}$	$2.49 \times 10^{+1}$	$2.49 \times 10^{+1}$
U1	(4/26)	2.84×10^{-6}	-5.81×10^{-7}	4.55×10^{-6}
W1		1.31×10^{-4}	1.26×10^{-4}	3.75×10^{-4}
U2	(8/26)	2.09×10^{-5}	-4.34×10^{-6}	3.63×10^{-5}
W2		1.11×10^{-4}	1.05×10^{-4}	3.35×10^{-4}
U3	(10/24)	5.38×10^{-6}	1.12×10^{-6}	2.08×10^{-4}
W3		1.02×10^{-4}	4.03×10^{-5}	1.03×10^{-4}
U4	(10/22)	4.17×10^{-6}	2.04×10^{-6}	2.42×10^{-4}
W4		1.18×10^{-4}	5.14×10^{-5}	1.69×10^{-4}
U5	(10/19)	-4.54×10^{-6}	-2.55×10^{-6}	3.17×10^{-4}
W5		1.09×10^{-4}	4.47×10^{-5}	1.20×10^{-3}
U6	(10/16)	-6.10×10^{-6}	-1.69×10^{-6}	-5.60×10^{-4}
W6		7.95×10^{-5}	4.41×10^{-5}	4.24×10^{-3}
U7	(8/14)	-1.81×10^{-5}	4.34×10^{-6}	-2.27×10^{-6}
W7		6.53×10^{-5}	1.22×10^{-4}	9.84×10^{-4}
U8	(4/14)	-2.45×10^{-6}	-3.49×10^{-6}	-6.83×10^{-6}
W8		7.42×10^{-5}	1.33×10^{-4}	1.01×10^{-3}

Table 6-6: Exit speeds (Darcy velocities in m/yr) out of Bentonite Barrier

		Case A (no cage)	Case B (with cage)	Case C (with cage + h.c. zone)
Time [yrs]		2190	2190	2190
Max Temperatures [°C]				
Sources	(3/21)	$4.51 \times 10^{+1}$	$4.50 \times 10^{+1}$	$4.50 \times 10^{+1}$
Cage	(16/21)	$2.00 \times 10^{+1}$	$2.00 \times 10^{+1}$	$2.00 \times 10^{+1}$
U1	(4/26)	1.94×10^{-6}	-4.36×10^{-7}	2.85×10^{-6}
W1		8.77×10^{-5}	8.46×10^{-5}	2.51×10^{-4}
U2	(8/26)	1.44×10^{-5}	-3.26×10^{-6}	2.37×10^{-5}
W2		7.47×10^{-5}	7.13×10^{-5}	2.24×10^{-4}
U3	(10/24)	3.30×10^{-6}	5.11×10^{-7}	1.38×10^{-4}
W3		6.58×10^{-5}	2.60×10^{-5}	6.74×10^{-5}
U4	(10/22)	2.65×10^{-6}	1.25×10^{-6}	1.60×10^{-4}
W4		7.64×10^{-5}	3.31×10^{-5}	1.12×10^{-4}
U5	(10/19)	-2.81×10^{-6}	-1.52×10^{-6}	2.10×10^{-4}
W5		7.08×10^{-5}	2.87×10^{-5}	8.04×10^{-4}
U6	(10/16)	-3.68×10^{-6}	-7.91×10^{-7}	-3.70×10^{-4}
W6		5.21×10^{-5}	3.00×10^{-5}	2.86×10^{-3}
U7	(8/14)	-1.22×10^{-5}	3.58×10^{-6}	1.20×10^{-6}
W7		4.41×10^{-5}	8.56×10^{-5}	6.60×10^{-4}
U8	(4/14)	-1.65×10^{-6}	-2.47×10^{-6}	-4.65×10^{-6}
W8		5.00×10^{-5}	9.16×10^{-5}	6.79×10^{-4}

Table 6-7: Exit speeds (Darcy velocities in m/yr) out of Bentonite Barrier

		Case A (no cage)	Case B (with cage)	Case C (with cage + h.c. zone)
Time [yrs]		3000	3000	3000
Max Temperatures ['C]				
Sources	(3/21)	$3.58 \times 10^{+1}$	$3.58 \times 10^{+1}$	$3.58 \times 10^{+1}$
Cage	(16/21)	$1.73 \times 10^{+1}$	$1.73 \times 10^{+1}$	$1.73 \times 10^{+1}$
U1	(4/26)	1.45×10^{-6}	-2.41×10^{-7}	2.13×10^{-6}
W1		6.44×10^{-5}	6.23×10^{-5}	1.85×10^{-4}
U2	(8/26)	1.08×10^{-5}	-2.32×10^{-6}	1.76×10^{-5}
W2		5.49×10^{-5}	5.25×10^{-5}	1.66×10^{-4}
U3	(10/24)	2.42×10^{-6}	4.12×10^{-7}	1.02×10^{-4}
W3		4.75×10^{-5}	1.90×10^{-5}	4.95×10^{-5}
U4	(10/22)	1.98×10^{-6}	9.69×10^{-7}	1.19×10^{-4}
W4		5.53×10^{-5}	2.42×10^{-5}	8.24×10^{-5}
U5	(10/19)	-1.99×10^{-6}	-1.06×10^{-6}	1.56×10^{-4}
W5		5.13×10^{-5}	2.10×10^{-5}	5.94×10^{-4}
U6	(10/16)	-2.59×10^{-6}	-5.07×10^{-7}	-2.74×10^{-4}
W6		3.77×10^{-5}	2.23×10^{-5}	2.12×10^{-3}
U7	(8/14)	-9.18×10^{-6}	2.79×10^{-6}	1.28×10^{-6}
W7		3.23×10^{-5}	6.43×10^{-5}	4.96×10^{-4}
U8	(4/14)	-1.24×10^{-6}	-1.82×10^{-6}	-3.42×10^{-6}
W8		3.67×10^{-5}	6.84×10^{-5}	5.03×10^{-4}

Table 6-8: Exit fluxes (Darcy velocities in m/yr) across Bentonite Barrier at time : 243.6 yrs from fuel unloading.

Monitor Point (see Fig. 5)	Comp	Case 1 (no cage + 0.81 MW)	Case 2 (with cage + 0.81 MW)	Case 3 (with cage + h.c. zone + 0.81 MW)	Case 4 (with cage + 1.13 MW)	Case 5 (no cage + 0.81 MW)	Case 6 (no cage + 0.6 MW)	Case 7 (with cage + 0.6 MW)	Case 8 (no cage + h.c. zone + 0.6 MW)
1	U	3.24×10^{-5}	3.11×10^{-5}	3.36×10^{-5}	4.28×10^{-5}	9.49×10^{-6}	3.95×10^{-5}	3.76×10^{-5}	3.66×10^{-5}
	W	3.05×10^{-3}	3.13×10^{-3}	3.51×10^{-3}	4.31×10^{-3}	1.14×10^{-3}	4.15×10^{-3}	4.36×10^{-3}	4.20×10^{-3}
2	U	4.02×10^{-4}	3.85×10^{-4}	4.18×10^{-4}	5.31×10^{-4}	1.22×10^{-4}	5.14×10^{-4}	4.91×10^{-4}	4.77×10^{-4}
	W	2.84×10^{-3}	2.92×10^{-3}	3.29×10^{-3}	4.02×10^{-3}	1.11×10^{-3}	4.09×10^{-3}	4.29×10^{-3}	4.14×10^{-3}
3	U	1.01×10^{-3}	9.63×10^{-4}	1.09×10^{-3}	1.33×10^{-3}	3.96×10^{-4}	1.78×10^{-3}	1.72×10^{-3}	1.66×10^{-3}
	W	1.83×10^{-3}	1.89×10^{-3}	2.23×10^{-3}	2.50×10^{-3}	9.49×10^{-4}	3.36×10^{-3}	3.54×10^{-3}	3.38×10^{-3}
4	U	2.04×10^{-3}	2.08×10^{-3}	2.46×10^{-3}	2.87×10^{-3}	8.40×10^{-4}	3.03×10^{-4}	4.13×10^{-4}	2.36×10^{-4}
	W	-2.43×10^{-4}	-8.66×10^{-5}	3.43×10^{-4}	-1.19×10^{-4}	7.96×10^{-5}	-1.74×10^{-4}	-4.89×10^{-5}	5.32×10^{-5}
5	U	-1.03×10^{-3}	-1.06×10^{-3}	2.21×10^{-4}	-1.46×10^{-3}	1.96×10^{-4}	1.94×10^{-4}	2.26×10^{-4}	-2.42×10^{-4}
	W	-9.59×10^{-4}	-7.01×10^{-4}	1.89×10^{-3}	-9.64×10^{-4}	-8.15×10^{-5}	-9.45×10^{-5}	2.68×10^{-5}	1.36×10^{-3}
6	U	-6.11×10^{-4}	-6.24×10^{-4}	-1.83×10^{-4}	-8.61×10^{-4}	-3.49×10^{-4}	-2.04×10^{-4}	-2.37×10^{-4}	-3.99×10^{-3}
	W	1.19×10^{-4}	2.13×10^{-4}	1.91×10^{-2}	2.95×10^{-4}	-2.90×10^{-5}	8.92×10^{-5}	3.03×10^{-5}	1.59×10^{-2}
7	U	-9.63×10^{-4}	-9.74×10^{-4}	-2.33×10^{-3}	-1.34×10^{-3}	-7.35×10^{-4}	-2.99×10^{-4}	-4.09×10^{-4}	-3.74×10^{-4}
	W	3.71×10^{-4}	2.79×10^{-4}	4.12×10^{-3}	3.84×10^{-4}	2.70×10^{-4}	3.31×10^{-4}	-1.85×10^{-4}	1.95×10^{-3}
8	U	-1.30×10^{-5}	-1.30×10^{-5}	-2.72×10^{-5}	-1.80×10^{-5}	-1.06×10^{-5}	-1.80×10^{-4}	-1.80×10^{-4}	-1.79×10^{-4}
	W	1.06×10^{-3}	1.07×10^{-3}	2.50×10^{-3}	1.47×10^{-3}	8.33×10^{-4}	3.35×10^{-3}	3.53×10^{-3}	3.75×10^{-3}
9	U	-3.49×10^{-6}	-3.48×10^{-6}	-4.50×10^{-6}	-4.81×10^{-6}	-3.27×10^{-6}	-4.93×10^{-5}	-4.88×10^{-5}	-4.85×10^{-5}
	W	1.16×10^{-3}	1.17×10^{-3}	2.68×10^{-3}	1.61×10^{-3}	9.27×10^{-4}	4.07×10^{-3}	4.27×10^{-3}	4.51×10^{-3}
10	U	-2.96×10^{-7}	-2.96×10^{-7}	-3.71×10^{-7}	-4.08×10^{-7}	-2.79×10^{-7}	-3.84×10^{-6}	-3.79×10^{-6}	-3.77×10^{-6}
	W	1.17×10^{-3}	1.18×10^{-3}	2.69×10^{-3}	1.63×10^{-3}	9.37×10^{-4}	4.13×10^{-3}	4.33×10^{-3}	4.57×10^{-3}

Total heat source strength at 40 yrs =

0.81 MW (cases 1, 2, 3)
1.13 MW (case 4)
0.81 MW (case 5)
0.60 MW (cases 6, 7, 8)

Table 6-9: Exit fluxes (Darcy velocities in m/yr) across Bentonite Barrier at time : 543.6 yrs from fuel unloading

Monitor Point (see Fig. 5)	Comp	Case 1 (no cage + 0.81 MW)	Case 2 (with cage + 0.81 MW)	Case 3 (with cage + h.c. zone + 0.81 MW)	Case 4 (with cage + 1.13 MW)	Case 5 (no cage + 0.81 MW)	Case 6 (no cage + 0.6 MW)	Case 7 (with cage + 0.6 MW)	Case 8 (no cage + h.c. zone + 0.6 MW)
1	U	2.30×10^{-5}	2.15×10^{-5}	2.34×10^{-5}	3.01×10^{-5}	6.83×10^{-6}	4.77×10^{-5}	4.47×10^{-5}	4.36×10^{-5}
	W	2.22×10^{-3}	2.26×10^{-3}	2.54×10^{-3}	3.14×10^{-3}	8.76×10^{-4}	5.30×10^{-3}	5.55×10^{-3}	5.38×10^{-3}
2	U	2.85×10^{-4}	2.67×10^{-4}	2.93×10^{-4}	3.71×10^{-4}	8.75×10^{-5}	6.26×10^{-4}	5.87×10^{-4}	5.72×10^{-4}
	W	2.07×10^{-3}	2.11×10^{-3}	2.39×10^{-3}	2.93×10^{-3}	8.56×10^{-4}	5.27×10^{-3}	5.52×10^{-3}	5.35×10^{-3}
3	U	7.15×10^{-4}	6.64×10^{-4}	7.57×10^{-4}	9.23×10^{-4}	2.87×10^{-4}	2.35×10^{-3}	2.25×10^{-3}	2.18×10^{-3}
	W	1.36×10^{-3}	1.38×10^{-3}	1.64×10^{-3}	1.91×10^{-3}	7.40×10^{-4}	4.83×10^{-3}	5.04×10^{-3}	4.86×10^{-3}
4	U	1.43×10^{-3}	1.45×10^{-3}	1.73×10^{-3}	2.01×10^{-3}	5.84×10^{-4}	8.72×10^{-5}	1.93×10^{-4}	-6.85×10^{-6}
	W	-1.12×10^{-4}	-5.48×10^{-5}	3.01×10^{-4}	-7.59×10^{-5}	1.18×10^{-4}	-2.69×10^{-4}	-1.19×10^{-4}	-1.12×10^{-5}
5	U	-7.47×10^{-4}	-7.67×10^{-4}	8.29×10^{-5}	-1.06×10^{-3}	1.29×10^{-4}	9.61×10^{-5}	1.21×10^{-4}	-3.85×10^{-4}
	W	-6.22×10^{-4}	-5.08×10^{-4}	1.81×10^{-3}	-7.05×10^{-4}	-1.11×10^{-5}	-7.95×10^{-5}	2.14×10^{-5}	1.41×10^{-3}
6	U	-4.23×10^{-4}	-4.29×10^{-4}	-1.88×10^{-4}	-5.96×10^{-4}	-2.43×10^{-4}	-9.92×10^{-5}	-1.25×10^{-4}	-3.76×10^{-3}
	W	1.38×10^{-4}	1.31×10^{-4}	1.52×10^{-2}	1.81×10^{-4}	3.11×10^{-5}	-7.62×10^{-5}	2.36×10^{-5}	1.39×10^{-2}
7	U	-6.63×10^{-4}	-6.63×10^{-4}	-1.59×10^{-3}	-9.22×10^{-4}	-5.06×10^{-4}	-7.97×10^{-5}	-1.85×10^{-4}	2.42×10^{-4}
	W	3.28×10^{-4}	2.14×10^{-4}	3.78×10^{-3}	2.97×10^{-4}	2.57×10^{-4}	-5.61×10^{-4}	-3.69×10^{-4}	1.88×10^{-5}
8	U	-9.16×10^{-6}	-9.09×10^{-6}	-1.87×10^{-5}	-1.26×10^{-5}	-7.53×10^{-6}	-1.89×10^{-4}	-1.88×10^{-4}	-1.86×10^{-4}
	W	8.09×10^{-4}	8.06×10^{-4}	1.82×10^{-3}	1.12×10^{-3}	6.54×10^{-4}	4.84×10^{-3}	5.05×10^{-3}	5.26×10^{-3}
9	U	-2.37×10^{-6}	-2.34×10^{-6}	-2.90×10^{-6}	-3.26×10^{-6}	-2.22×10^{-6}	-4.19×10^{-5}	-4.10×10^{-5}	-4.06×10^{-5}
	W	8.83×10^{-4}	8.81×10^{-4}	1.94×10^{-3}	1.22×10^{-3}	7.21×10^{-4}	5.28×10^{-3}	5.53×10^{-3}	5.75×10^{-3}
10	U	-2.01×10^{-7}	-1.99×10^{-7}	-2.39×10^{-7}	-2.78×10^{-7}	-1.89×10^{-7}	-3.24×10^{-6}	-3.17×10^{-6}	-8.14×10^{-6}
	W	8.90×10^{-4}	8.88×10^{-4}	1.95×10^{-3}	1.23×10^{-3}	7.28×10^{-4}	5.31×10^{-3}	5.56×10^{-3}	5.78×10^{-3}

Total heat source strength at 40 yrs = 0.81 MW (cases 1, 2, 3)
1.13 MW (case 4)
0.81 MW (case 5)
0.60 MW (cases 6, 7, 8)

Table 6-10: Exit fluxes (Darcy velocities in m/yr) across Bentonite Barrier at time : 1444 yrs from fuel unloading

Monitor Point (see Fig. 5)	Comp	Case 1 (no cage + 0.81 MW)	Case 2 (with cage + 0.81 MW)	Case 3 (with cage + h.c. zone + 0.81 MW)	Case 4 (with cage + 1.13 MW)	Case 5 (no cage + 0.81 MW)	Case 6 (no cage + 0.6 MW)	Case 7 (with cage + 0.6 MW)	Case 8 (no cage + h.c. zone + 0.6 MW)
1	U	9.06×10^{-6}	8.34×10^{-6}	9.15×10^{-6}	1.16×10^{-5}	2.75×10^{-6}	2.28×10^{-5}	2.08×10^{-5}	2.07×10^{-5}
	W	8.81×10^{-4}	8.98×10^{-4}	1.01×10^{-3}	1.25×10^{-3}	3.57×10^{-4}	2.58×10^{-3}	2.71×10^{-3}	2.63×10^{-3}
2	U	1.13×10^{-4}	1.04×10^{-4}	1.13×10^{-4}	1.44×10^{-4}	3.53×10^{-5}	2.99×10^{-4}	2.79×10^{-4}	2.72×10^{-4}
	W	8.23×10^{-4}	8.39×10^{-4}	9.54×10^{-4}	1.17×10^{-3}	3.50×10^{-4}	2.58×10^{-3}	2.71×10^{-3}	2.63×10^{-3}
3	U	2.82×10^{-4}	2.56×10^{-4}	2.93×10^{-4}	3.56×10^{-4}	1.16×10^{-4}	1.16×10^{-3}	1.10×10^{-3}	1.07×10^{-3}
	W	5.42×10^{-4}	5.52×10^{-4}	6.57×10^{-4}	7.69×10^{-4}	3.05×10^{-4}	2.46×10^{-3}	2.56×10^{-3}	2.48×10^{-3}
4	U	5.61×10^{-4}	5.64×10^{-4}	6.78×10^{-4}	7.86×10^{-4}	2.28×10^{-4}	3.52×10^{-6}	5.50×10^{-5}	-3.61×10^{-5}
	W	-4.09×10^{-5}	-2.19×10^{-5}	1.25×10^{-4}	-3.05×10^{-4}	4.89×10^{-5}	-1.44×10^{-4}	-6.71×10^{-5}	-1.87×10^{-5}
5	U	-2.95×10^{-4}	-3.03×10^{-4}	2.29×10^{-5}	-4.22×10^{-4}	4.93×10^{-5}	2.94×10^{-5}	4.07×10^{-5}	-1.88×10^{-4}
	W	-2.44×10^{-4}	-2.05×10^{-4}	7.74×10^{-4}	-2.85×10^{-4}	-4.98×10^{-6}	-4.18×10^{-5}	5.50×10^{-6}	6.29×10^{-4}
6	U	-1.65×10^{-4}	-1.67×10^{-4}	-8.21×10^{-5}	-2.32×10^{-4}	-9.52×10^{-5}	-3.15×10^{-5}	-4.39×10^{-5}	-1.63×10^{-3}
	W	5.51×10^{-5}	4.54×10^{-5}	6.16×10^{-3}	6.31×10^{-5}	1.30×10^{-5}	-4.02×10^{-5}	6.58×10^{-6}	5.85×10^{-3}
7	U	-2.57×10^{-4}	-2.57×10^{-4}	-6.18×10^{-4}	-3.58×10^{-4}	-1.97×10^{-4}	-2.37×10^{-6}	-5.33×10^{-5}	1.43×10^{-4}
	W	1.35×10^{-4}	8.65×10^{-5}	1.61×10^{-3}	1.20×10^{-4}	1.07×10^{-4}	-2.95×10^{-4}	-1.96×10^{-4}	8.12×10^{-4}
8	U	-3.60×10^{-6}	-3.55×10^{-5}	-7.26×10^{-6}	-4.94×10^{-6}	2.97×10^{-6}	-8.31×10^{-5}	-8.25×10^{-5}	-8.17×10^{-5}
	W	3.30×10^{-4}	3.28×10^{-4}	7.25×10^{-4}	4.57×10^{-4}	2.70×10^{-4}	2.46×10^{-3}	2.56×10^{-3}	2.65×10^{-3}
9	U	-9.18×10^{-7}	-9.03×10^{-6}	-1.10×10^{-6}	-1.26×10^{-6}	-8.58×10^{-7}	-1.66×10^{-5}	-1.16×10^{-6}	-1.59×10^{-5}
	W	3.59×10^{-4}	3.57×10^{-4}	7.74×10^{-4}	4.98×10^{-4}	2.96×10^{-4}	2.58×10^{-3}	2.70×10^{-3}	2.80×10^{-3}
10	U	-7.80×10^{-8}	-7.70×10^{-8}	-9.09×10^{-8}	-1.08×10^{-7}	-7.34×10^{-8}	-1.28×10^{-6}	-1.23×10^{-6}	-1.23×10^{-6}
	W	3.61×10^{-4}	3.60×10^{-4}	7.77×10^{-4}	5.01×10^{-4}	2.98×10^{-4}	2.58×10^{-3}	2.71×10^{-3}	2.80×10^{-3}

Total heat source strength at 40 yrs =

0.81 MW (cases 1, 2, 3)
1.13 MW (case 4)
0.81 MW (case 5)
0.60 MW (cases 6, 7, 8)

Table 6-11: Exit fluxes (Darcy velocities in m/yr) across Bentonite Barrier at time : 2344 yrs from fuel unloading

Monitor Point (see Fig. 5)	Comp	Case 1 (no cage + 0.81 MW)	Case 2 (with cage + 0.81 MW)	Case 3 (with cage + h.c. zone + 0.81 MW)	Case 4 (with cage + 1.13 MW)	Case 5 (no cage + 0.81 MW)	Case 6 (no cage + 0.6 MW)	Case 7 (with cage + 0.6 MW)	Case 8 (no cage + h.c. zone + 0.6 MW)
1	U	5.47×10^{-6}	5.04×10^{-6}	5.50×10^{-6}	6.95×10^{-6}	1.68×10^{-6}	1.41×10^{-5}	1.31×10^{-5}	1.27×10^{-5}
	W	5.32×10^{-4}	5.43×10^{-4}	6.13×10^{-4}	7.56×10^{-4}	2.17×10^{-4}	1.60×10^{-3}	1.68×10^{-3}	1.63×10^{-3}
2	U	6.80×10^{-5}	6.23×10^{-5}	6.83×10^{-5}	8.69×10^{-5}	2.15×10^{-5}	1.85×10^{-4}	1.72×10^{-4}	1.68×10^{-4}
	W	4.96×10^{-4}	5.07×10^{-4}	5.77×10^{-4}	7.07×10^{-4}	2.12×10^{-4}	1.60×10^{-3}	1.68×10^{-3}	1.63×10^{-3}
3	U	1.71×10^{-4}	1.54×10^{-4}	1.76×10^{-4}	2.14×10^{-4}	7.11×10^{-5}	7.21×10^{-4}	6.85×10^{-4}	6.67×10^{-4}
	W	3.27×10^{-4}	3.34×10^{-4}	3.98×10^{-4}	4.65×10^{-4}	1.85×10^{-4}	1.54×10^{-3}	1.61×10^{-3}	1.56×10^{-3}
4	U	3.38×10^{-4}	3.40×10^{-4}	4.09×10^{-4}	4.74×10^{-4}	1.37×10^{-4}	-2.38×10^{-6}	3.04×10^{-5}	-2.56×10^{-5}
	W	-2.60×10^{-5}	-1.35×10^{-5}	7.63×10^{-5}	-1.89×10^{-5}	2.79×10^{-5}	-9.25×10^{-5}	-4.29×10^{-5}	-1.32×10^{-5}
5	U	-1.78×10^{-4}	-1.83×10^{-4}	1.33×10^{-4}	-2.54×10^{-4}	2.97×10^{-5}	1.66×10^{-5}	2.37×10^{-5}	-1.17×10^{-4}
	W	-1.49×10^{-4}	-1.24×10^{-4}	4.74×10^{-4}	-1.73×10^{-4}	-4.77×10^{-6}	-2.76×10^{-5}	2.53×10^{-6}	3.85×10^{-4}
6	U	-9.93×10^{-5}	-1.00×10^{-4}	-5.03×10^{-5}	-1.40×10^{-4}	-5.73×10^{-5}	-1.79×10^{-5}	-2.58×10^{-5}	-9.97×10^{-4}
	W	3.17×10^{-5}	2.63×10^{-5}	3.74×10^{-3}	3.61×10^{-5}	6.34×10^{-6}	-2.64×10^{-5}	3.16×10^{-6}	3.54×10^{-3}
7	U	-1.55×10^{-4}	-1.55×10^{-4}	-3.72×10^{-4}	-2.15×10^{-4}	-1.18×10^{-4}	2.74×10^{-6}	-2.97×10^{-5}	9.11×10^{-5}
	W	8.06×10^{-5}	5.24×10^{-5}	9.88×10^{-4}	7.30×10^{-5}	6.39×10^{-5}	-1.87×10^{-4}	-1.24×10^{-4}	4.95×10^{-4}
8	U	-2.17×10^{-6}	-2.14×10^{-6}	-4.38×10^{-6}	-2.98×10^{-6}	-1.79×10^{-6}	-5.02×10^{-5}	-4.99×10^{-5}	4.94×10^{-5}
	W	2.01×10^{-4}	2.00×10^{-4}	4.40×10^{-4}	2.78×10^{-4}	1.65×10^{-4}	1.54×10^{-3}	1.60×10^{-3}	1.66×10^{-3}
9	U	-5.53×10^{-7}	5.43×10^{-7}	-6.61×10^{-7}	-7.57×10^{-7}	-5.17×10^{-7}	-9.74×10^{-6}	-9.45×10^{-6}	-9.33×10^{-6}
	W	2.18×10^{-4}	2.17×10^{-4}	4.69×10^{-4}	3.03×10^{-4}	1.80×10^{-4}	1.60×10^{-3}	1.68×10^{-3}	1.73×10^{-3}
10	U	-4.70×10^{-8}	-4.63×10^{-8}	-5.46×10^{-8}	-6.48×10^{-8}	-4.43×10^{-8}	-7.50×10^{-5}	-7.29×10^{-7}	-7.18×10^{-7}
	W	2.19×10^{-4}	2.19×10^{-4}	4.70×10^{-4}	3.05×10^{-4}	1.81×10^{-4}	1.60×10^{-3}	1.68×10^{-3}	1.74×10^{-3}

Total heat source strength at 40 yrs = 0.81 MW (cases 1, 2, 3)
1.13 MW (case 4)
0.81 MW (case 5)
0.60 MW (cases 6, 7, 8)

Table 6-12: Exit fluxes (Darcy velocities in m/yr) across Bentonite Barrier at time : 3000 yrs from fuel unloading

Monitor Point (see Fig. 5)	Comp	Case 1 (no cage + 0.81 MW)	Case 2 (with cage + 0.81 MW)	Case 3 (with cage + h.c. zone + 0.81 MW)	Case 4 (with cage + 1.13 MW)	Case 5 (no cage + 0.81 MW)	Case 6 (no cage + 0.6 MW)	Case 7 (with cage + 0.6 MW)	Case 8 (no cage + h.c. zone + 0.6 MW)
1	U	4.31×10^{-6}	3.94×10^{-6}	4.40×10^{-6}	5.56×10^{-6}	1.33×10^{-6}	1.11×10^{-5}	1.03×10^{-5}	1.02×10^{-5}
	W	4.18×10^{-4}	4.27×10^{-4}	4.82×10^{-4}	5.95×10^{-4}	1.70×10^{-4}	1.26×10^{-3}	1.33×10^{-3}	1.29×10^{-3}
2	U	5.35×10^{-5}	4.91×10^{-5}	5.37×10^{-5}	6.82×10^{-5}	1.70×10^{-5}	1.46×10^{-4}	1.36×10^{-4}	1.32×10^{-4}
	W	3.90×10^{-4}	3.99×10^{-4}	4.54×10^{-4}	5.56×10^{-4}	1.67×10^{-4}	1.26×10^{-3}	1.32×10^{-3}	1.29×10^{-3}
3	U	1.34×10^{-4}	1.21×10^{-4}	1.39×10^{-4}	1.69×10^{-4}	5.62×10^{-5}	5.68×10^{-4}	5.40×10^{-4}	5.26×10^{-4}
	W	2.57×10^{-4}	2.63×10^{-4}	3.13×10^{-4}	3.66×10^{-4}	1.46×10^{-4}	1.21×10^{-3}	1.27×10^{-3}	1.23×10^{-3}
4	U	2.66×10^{-4}	2.68×10^{-4}	3.22×10^{-4}	3.73×10^{-4}	1.08×10^{-4}	-1.91×10^{-6}	2.44×10^{-5}	-1.99×10^{-5}
	W	-2.11×10^{-5}	-1.07×10^{-5}	6.00×10^{-5}	-1.50×10^{-5}	2.13×10^{-5}	-7.36×10^{-5}	-3.40×10^{-5}	-1.05×10^{-5}
5	U	-1.40×10^{-4}	-1.43×10^{-4}	1.09×10^{-5}	-2.00×10^{-4}	2.34×10^{-5}	1.35×10^{-5}	1.92×10^{-5}	-9.17×10^{-5}
	W	-1.18×10^{-4}	-9.81×10^{-5}	3.74×10^{-4}	-1.36×10^{-4}	-4.44×10^{-6}	-2.23×10^{-5}	1.87×10^{-6}	3.04×10^{-4}
6	U	-7.82×10^{-5}	-7.91×10^{-5}	-3.95×10^{-5}	-1.10×10^{-4}	-4.51×10^{-5}	-1.34×10^{-5}	-1.98×10^{-5}	-7.86×10^{-4}
	W	2.42×10^{-5}	2.06×10^{-5}	2.94×10^{-3}	2.89×10^{-5}	4.32×10^{-6}	-2.14×10^{-5}	2.27×10^{-6}	2.79×10^{-3}
7	U	-1.22×10^{-4}	-1.22×10^{-4}	-2.93×10^{-4}	-1.70×10^{-4}	-9.30×10^{-5}	3.42×10^{-6}	-2.26×10^{-5}	7.28×10^{-5}
	W	6.28×10^{-5}	4.13×10^{-5}	7.78×10^{-4}	5.76×10^{-5}	4.97×10^{-5}	-1.49×10^{-4}	-9.85×10^{-5}	3.90×10^{-4}
8	U	-1.71×10^{-6}	-1.69×10^{-6}	-3.45×10^{-6}	-2.35×10^{-6}	-1.41×10^{-6}	-3.95×10^{-5}	-3.92×10^{-5}	-3.88×10^{-5}
	W	1.58×10^{-4}	1.58×10^{-4}	3.46×10^{-4}	2.20×10^{-4}	1.30×10^{-4}	1.22×10^{-3}	1.27×10^{-3}	1.32×10^{-3}
9	U	-4.36×10^{-7}	-4.28×10^{-7}	-5.21×10^{-7}	-5.98×10^{-7}	-4.08×10^{-7}	-7.62×10^{-6}	-7.39×10^{-6}	-7.30×10^{-6}
	W	1.72×10^{-4}	1.71×10^{-4}	3.69×10^{-4}	2.39×10^{-4}	1.42×10^{-4}	1.26×10^{-3}	1.33×10^{-3}	1.37×10^{-3}
10	U	-3.71×10^{-6}	-3.59×10^{-6}	-4.28×10^{-6}	-5.09×10^{-6}	-3.49×10^{-6}	-5.86×10^{-7}	-5.68×10^{-7}	-5.67×10^{-7}
	W	1.73×10^{-4}	1.72×10^{-4}	3.71×10^{-4}	2.40×10^{-4}	1.43×10^{-4}	1.27×10^{-3}	1.33×10^{-3}	1.38×10^{-3}

Total heat source strength at 40 yrs =

0.81 MW (cases 1, 2, 3)
1.13 MW (case 4)
0.81 MW (case 5)
0.60 MW (cases 6, 7, 8)

7. Conclusions and Recommendations

The results presented in the previous chapter demonstrate the great importance of the hydraulic conductivity of the bentonite/sand barrier and of the rock mass inside this barrier. They also indicate the almost proportional dependence of Darcy velocity on the temperature and thus on the thermal load in the repository. The influence of the hydraulic cage upon internally generated buoyant, convective motion is only minor.

The presence of a 10 meter thick highly conductive zone as simulated in Cases C, 3 and 8 has a noticeable effect upon the circulation patterns. Such a zone, passing directly below the storage region is crossed by the bentonite barrier as well as by the hydraulic cage and facilitates the circulation of fluid in the major convective cell in the space between diffusive barrier and hydraulic cage. It is through the high conductivity zone, when it is present, that most of the fluid is drawn into the space within the hydraulic cage. Thus the mixing and removal of solutes which cross the bentonite is promoted by the presence of such a feature. On the other hand, a comparison of the tabulated results in Chapter 6 of the cases with and without the high conductivity zone reveals the redistribution of the flows at the monitoring points. Although the changes close to the zone tend to be large, the integrated net flow across the bentonite barrier changes very little.

The calculations have been pursued out to a time of 3000 years. From the tables and figures presented in the previous chapter it has been observed that the temperatures and flow velocities induced by the heat-generating waste follow similar patterns. The hundred year period of controlled cooling has a very strong limiting effect. The spent fuel however still exhibits such a strong heat release rate at the end of this period, that rather high temperatures still occur afterwards at the centre of the repository. The induced circulations reflect closely the form of the temperature curve. The motion is at its most intense at about 300 years (highest temperatures about 200 years) and after 3000 years has decayed again by approximately one order of magnitude.

Within the bentonite shell the flow speeds at early times tend to be somewhat higher than outside. Peak differences of a factor of four can be detected around the time of closure. With the spreading of the temperature disturbance as time increases the induced velocities become rather uniform over the whole near field.

The effects of the very highly conductive hydraulic cage are twofold. First of all, it connects the regions above and below the heat source. Very high hydraulic velocities are induced in the vertical tubes (up to thousands of metres per year). However the net quantity of fluid transported is small, so that its thermal influence on the core of the convective cell as it passes through the waste storage volume is minimal. It may be seen upon examination of the tables 6-1 to 6-8 that just a slight redistribution of the transport velocities across the bentonite barrier occurs.

The reason for this is the second effect of the cage's presence, which is to provide a sharp separation of the upwards and downwards-moving flows induced in the major convective cell. The high hydraulic conductivity of the cage renders it sensitive to small pressure gradients. Consequently a number of small mechanically induced convection cells build up, driven alternately by the ascending flow within the cage and the descending flow outside.

Whereas this motion, which is also observed to vary with time, is intense and liable to cause mixing of any solute crossing it in the major circulation pattern, it does not radically affect the latter.

The possible effect of dispersion by motion in the cage of solute emerging from the near field should be borne in mind in a migration analysis.

The geometrical simplifications undertaken in the interests of computational time have not prevented the essential features of the WP-Cave from being simulated in a satisfactory manner.

It may be seen that the hydraulic cage, designed to prevent groundwater from seeping through the near field of the repository has a very minor effect upon flows generated by thermal buoyancy forces within the near field itself. The axisymmetric model represents adequately the situation within a well-designed hydraulic cage, in that no lateral groundwater motion is represented. Thus the influence of buoyancy-induced advective migration added to the pure diffusion, which would provide the sole migration mechanism within this enclosed volume if the heat source were not present, may now be assessed.

The potential sensitivity of the repository to a hydraulically highly conductive feature is a cause for concern and underlines the need for site qualification. A sensitivity study for establishing the effect of various, typical hydraulic inhomogenities at a range of distances and positions relative to a repository situated in a passing groundwater flow would provide useful background information for this procedure.

The temperatures generated within the waste storage volume of this compact repository unit are high, particularly under the originally proposed thermal loading, presented here in Cases A, B, C and 4. Despite the fact that the total heat generation rate is respected, the axial symmetry of the model contributes slightly to these high temperatures, since even in the refined, second stage model the discrete storage channels are smeared into circular discs of greater volume. Reducing the initial heat load diminishes the peak temperature in almost linear proportionality.

8. Nomenclature

Variables and Coefficients used in the main text and in the appendices

a_b	Volumetric expansion coefficient of bulk soild [K^{-1}]
a_f	Volumetric expansion coefficient of fluid [K^{-1}]
a_m	Coefficients in the heat source polynomial expression
a_s	Volumetric expansion coefficient of solid portion alone [K^{-1}]
b_m	Coefficients in the polynomial fit to viscosity
C	Specific heat [J kg^{-1} K^{-1}]
g	Acceleration due to gravity [m s^{-2}]
h	Piezometric head, potential [m]
k	Thermal conductivity [W m^{-1} K^{-1}]
K	Hydraulic conductivity [m s^{-1}]
K_b	Bulk modulus of drained solid matrix [Pa]
K_f	Bulk modulus of the pore fluid [Pa]
K_s	Bulk modulus of the solid portion alone [Pa]
M	Viscosity ratio, μ_r/μ [-]
n	Porosity [-]
p	Pressure [Pa]
Q_0	Initial heat source intensity/ton $_U$ [W]
R	Density deficit (1 - ρ_r/ρ) [-]
S_m	Mean stress level [Pa]
S_p	Pressure dependent storage coefficient [Kg m^{-3} Pa^{-1}]
S_{th}	Temperature dependent storage coefficient [kg m^{-3} K^{-1}]
S^T	Thermal energy source strength [W m^{-3}]
t	Time [s]
T	Temperature [K]
u	Horizontal average pore water velocity [m s^{-1}]
U	Horizontal Darcy velocity [m s^{-1}]
v	Specific volume [[m^3 kg^{-1}]
w	Vertical average pore water velocity [m s^{-1}]
W	Vertical Darcy velocity [m s^{-1}]
x	Horizontal distance [m]
z	Vertical distance [m]
α	Biot's constant [-]

β	Compressibility = (bulk modulus)$^{-1}$ [Pa^{-1}]
μ	Viscosity [kg m^{-1} s^{-1}]
ρ	Density [kg m^{-3}]
θ	Temperature [K]

Subscripts

f, l	fluid or liquid property
i, j	referring to generalised cartesian coordinates
r	reference value
s	solid property

9. Bibliography

1. Hopkirk R.J.: "TROUGH-2DP (Transport of Radioactive Outflows in Underground Hydrology, 2 Dimensions, Porous Media), Users' Handbook and Theoretical Description, Revision 4"; POLYDYNAMICS LIMITED, Zürich, April 1987

2. Bear J.: Hydraulics of Groundwater, McGraw Hill, 1979

3. Dawson D.M. and Briggs A.: Prediction of the thermal conductivity of insulation materials, Journal of Materials Science, Vol. 16, 1981, pp. 3346 - 3356

4. Boliden WP- Contech AB: "NAK WP-Cave Project. Report on the Research and Development Stage May 1984 to October 1985"; Report Nr. SKN 16, SKN Stockholm, Nov. 1985

5. Schmidt E. and Grigull U. (eds): Properties of Water and Stream in S.I. Units, Springer Verlag, 1979

FIGURES

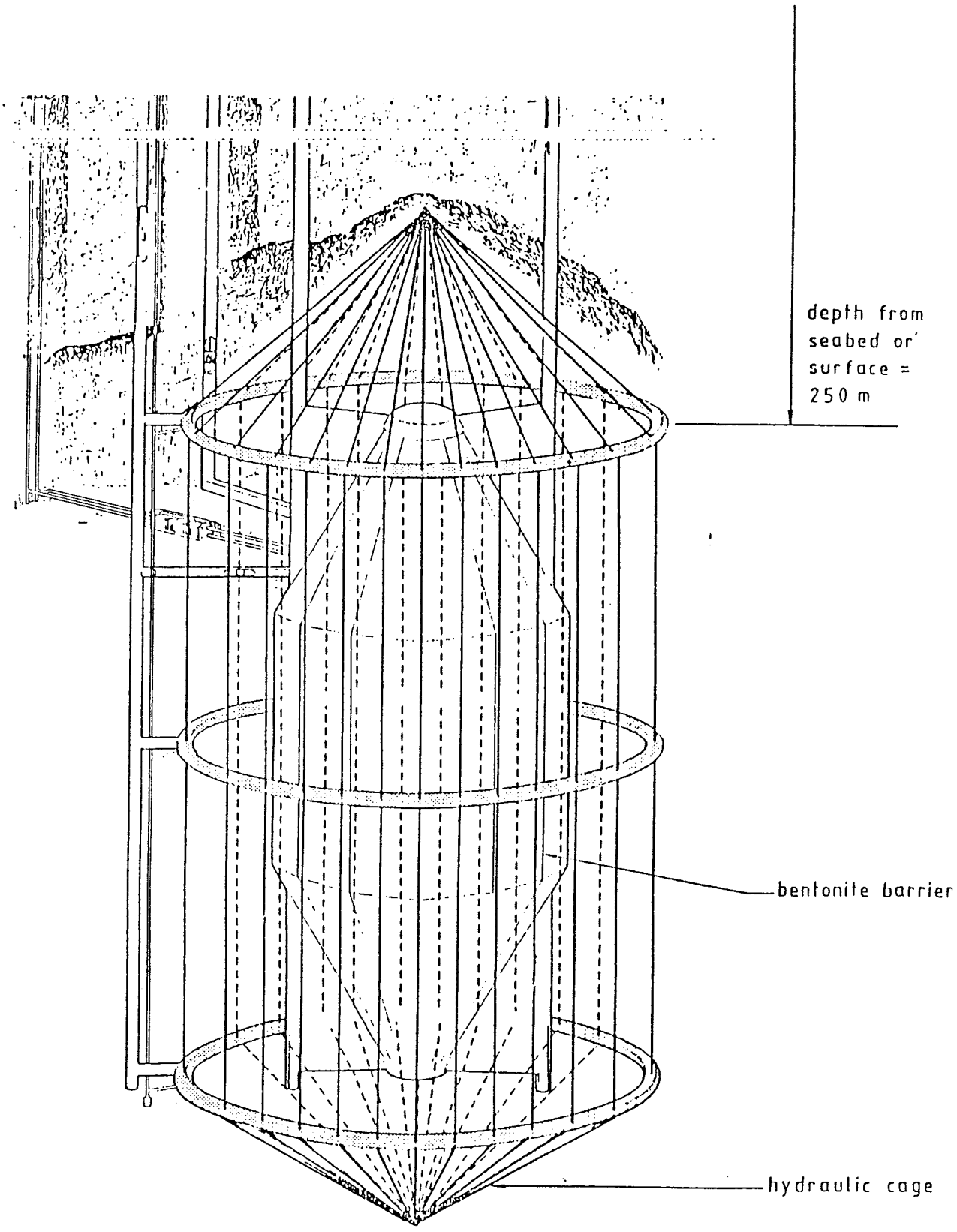

Figure 1: Overview of the System Geometry

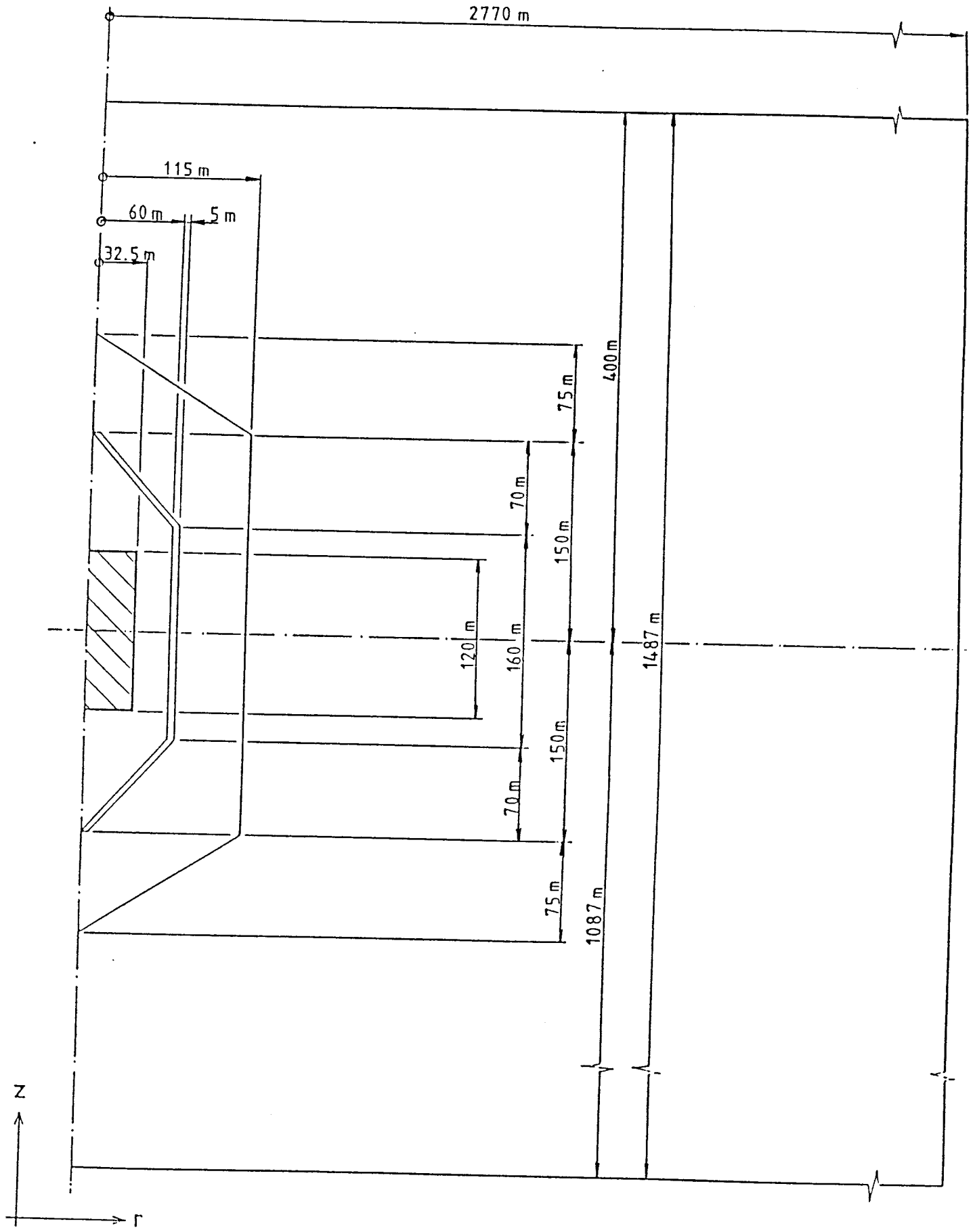

Figure 2: Model Geometry and Principal Dimensions

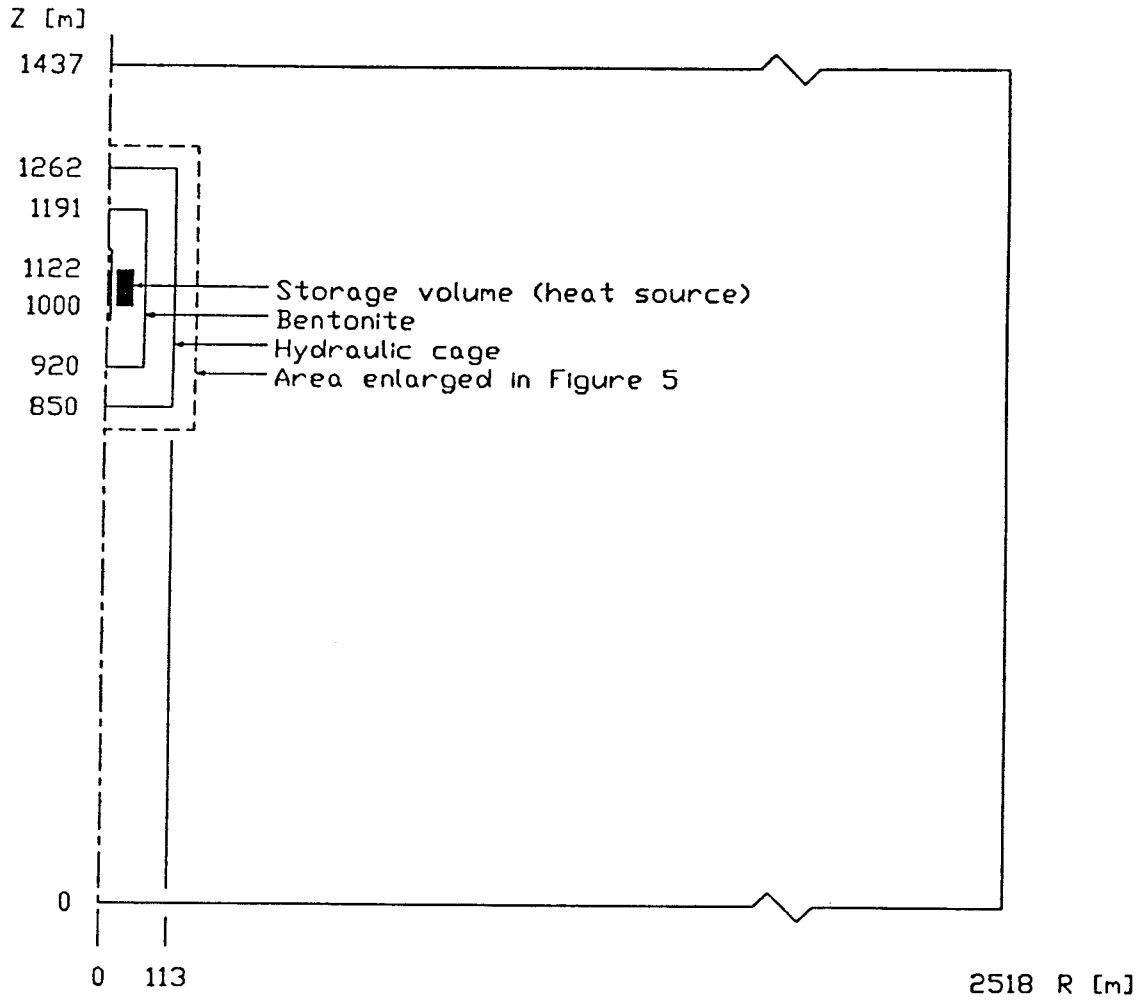

Figure 3: Simplified Geometrical Arrangement

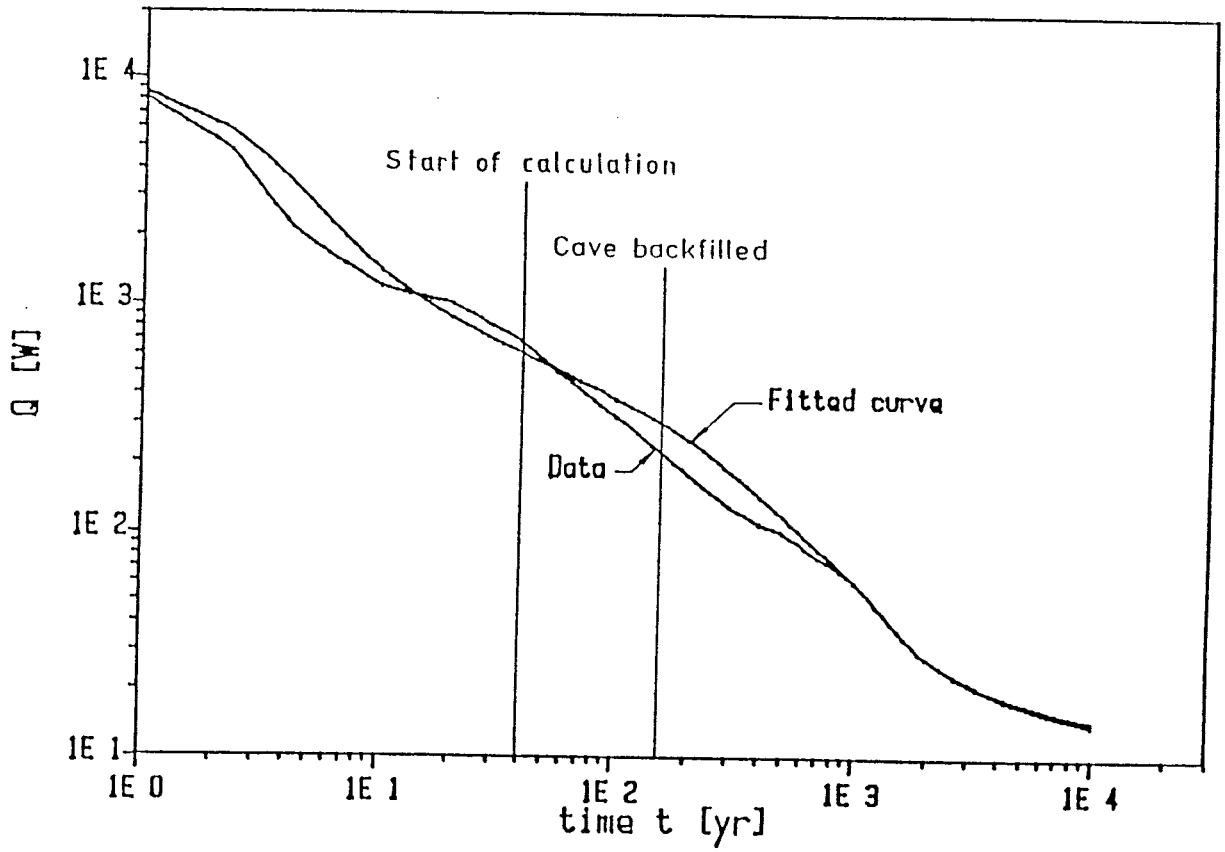

Figure 4: Heat Release Rates

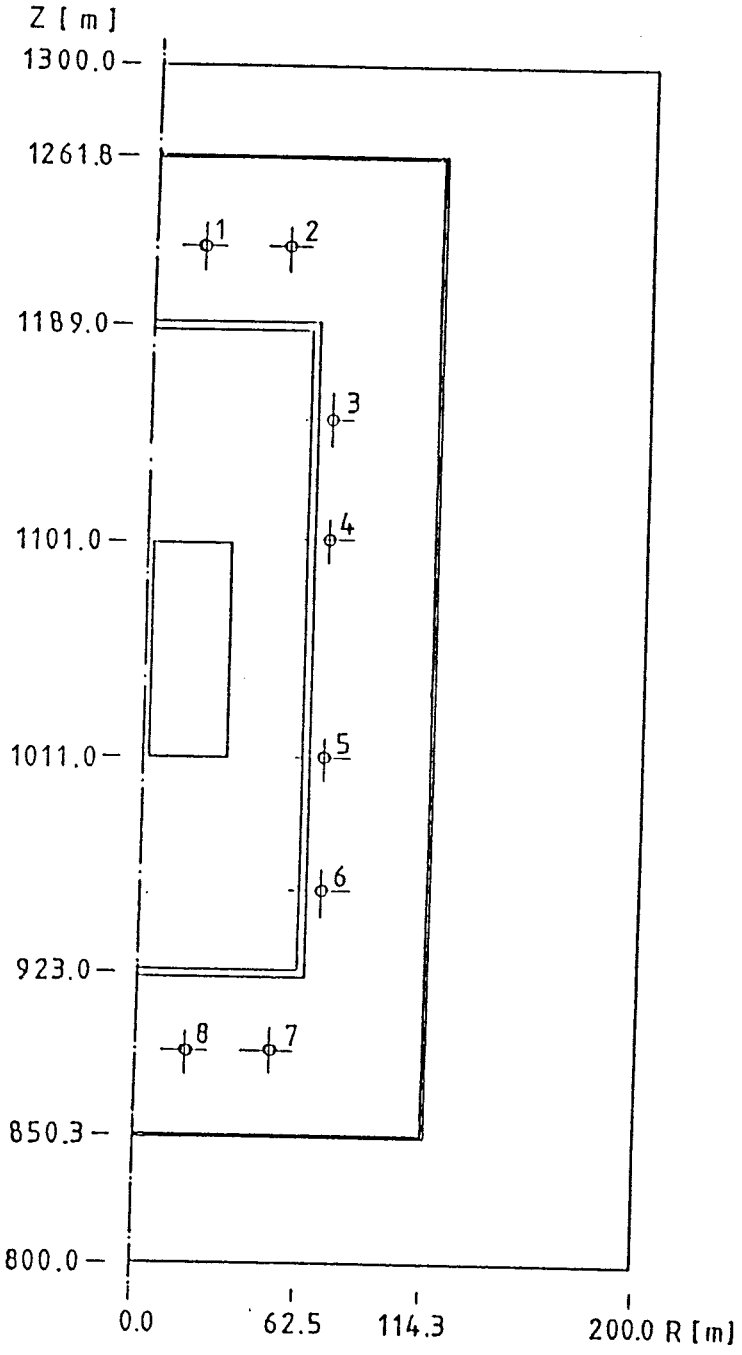

Figure 5a: Positions of the characteristic cells for the stage 1 calculation

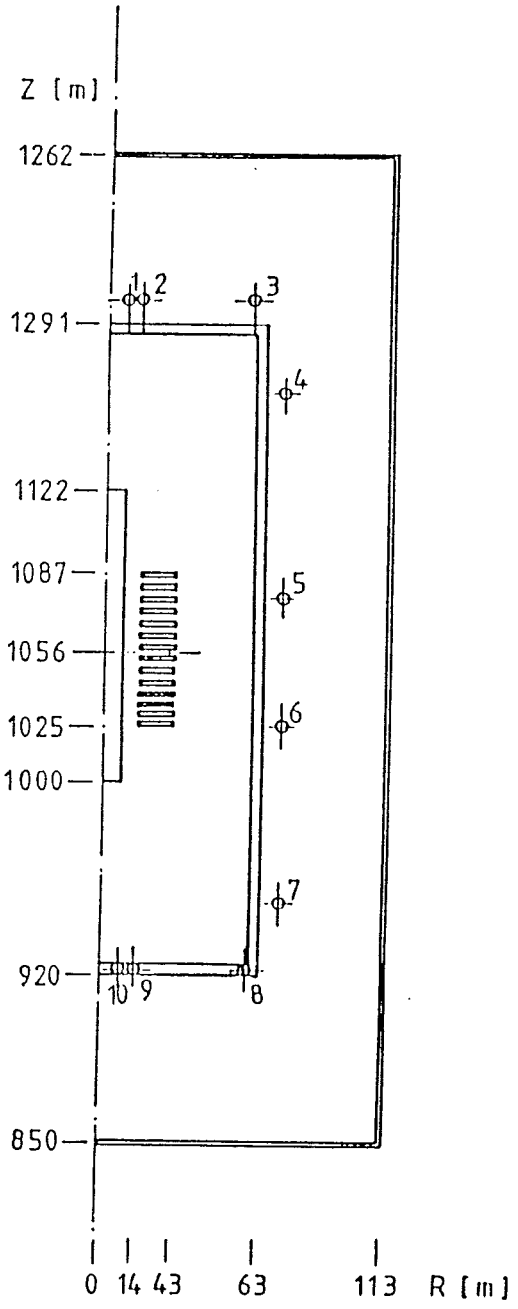

Figure 5b: Positions of the characteristic cells for the stage 2 calculation

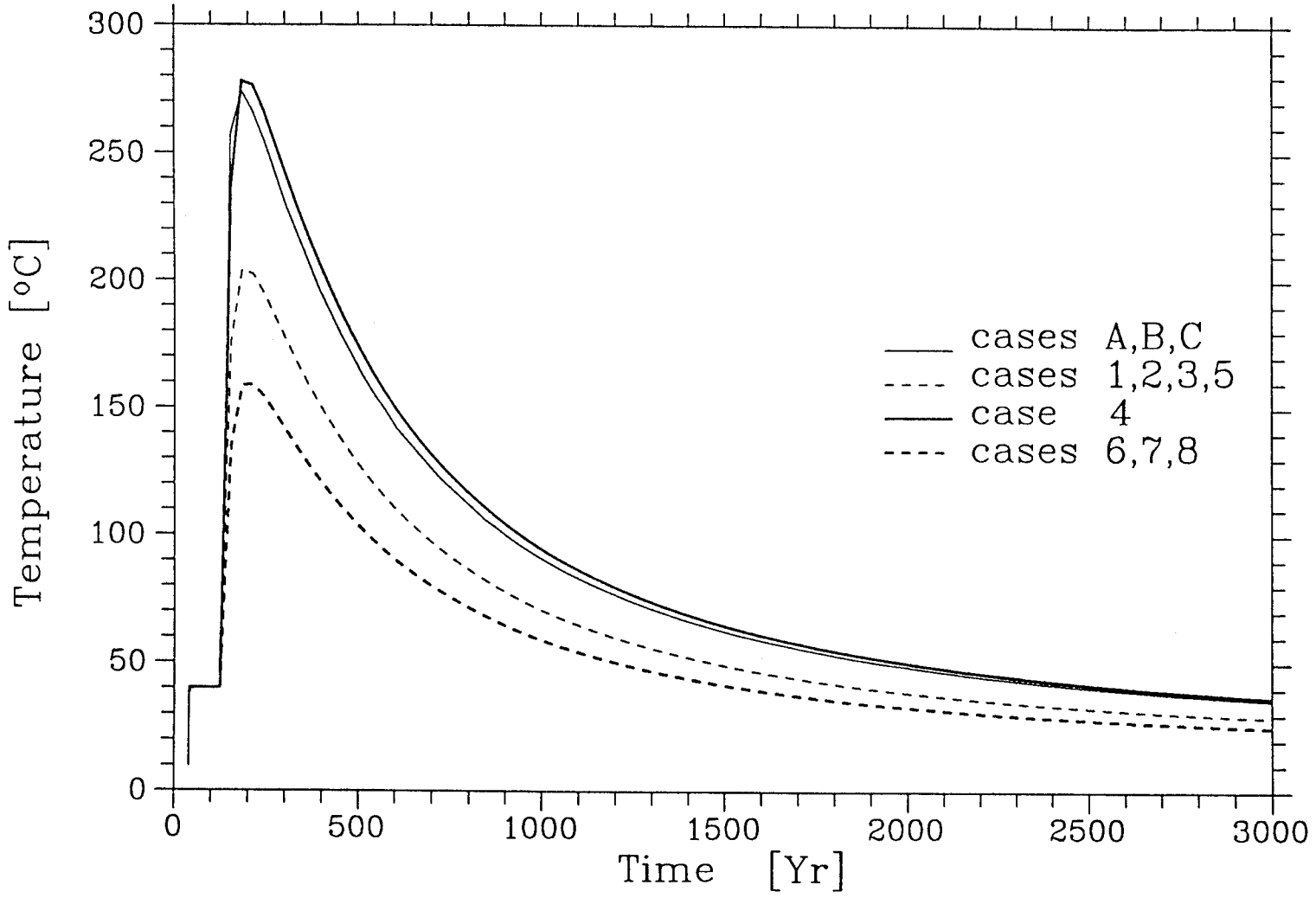

Figure 6: Temperature time history at hottest point in source region

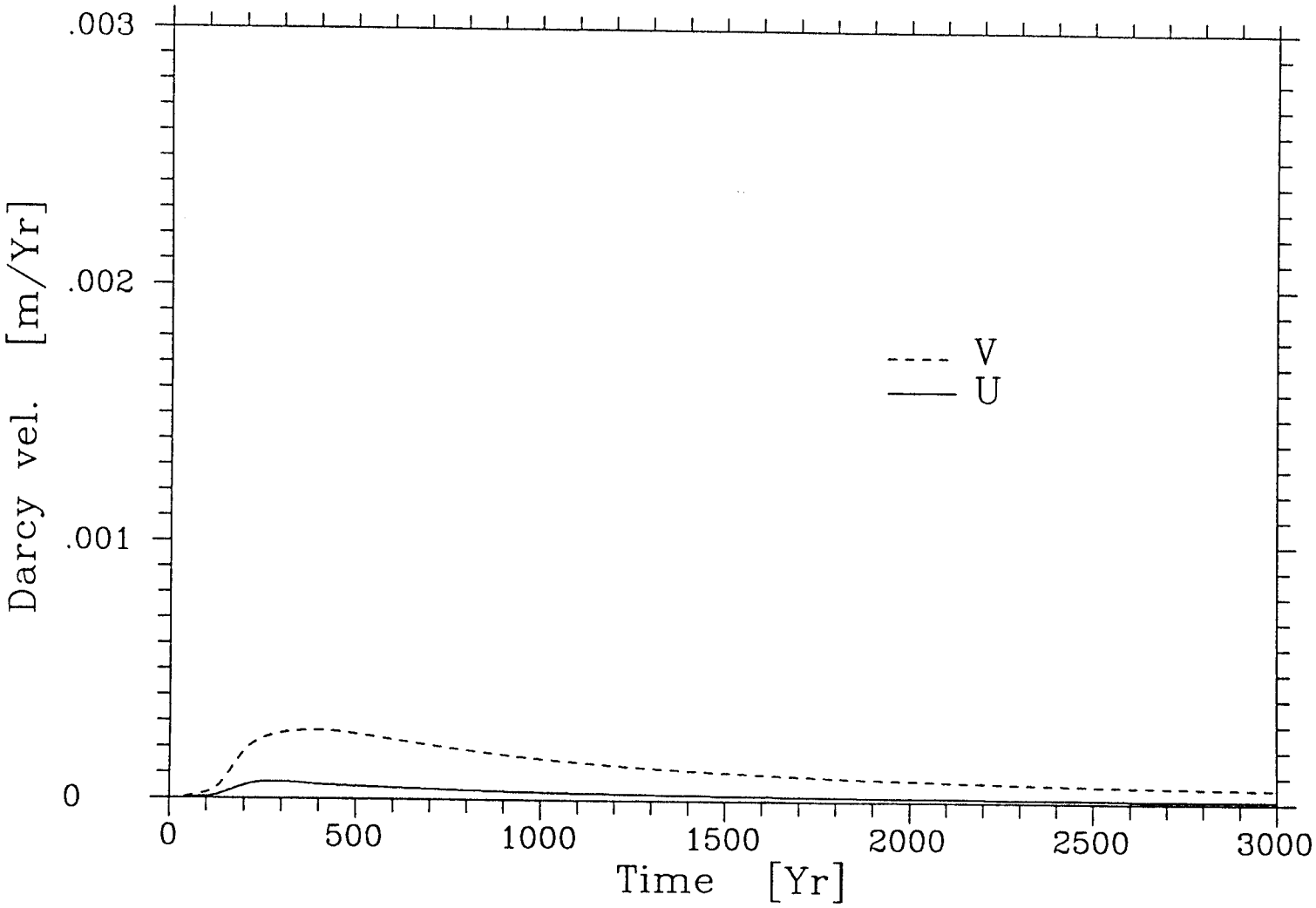

Figure 7: Velocity components at point 2 - case A

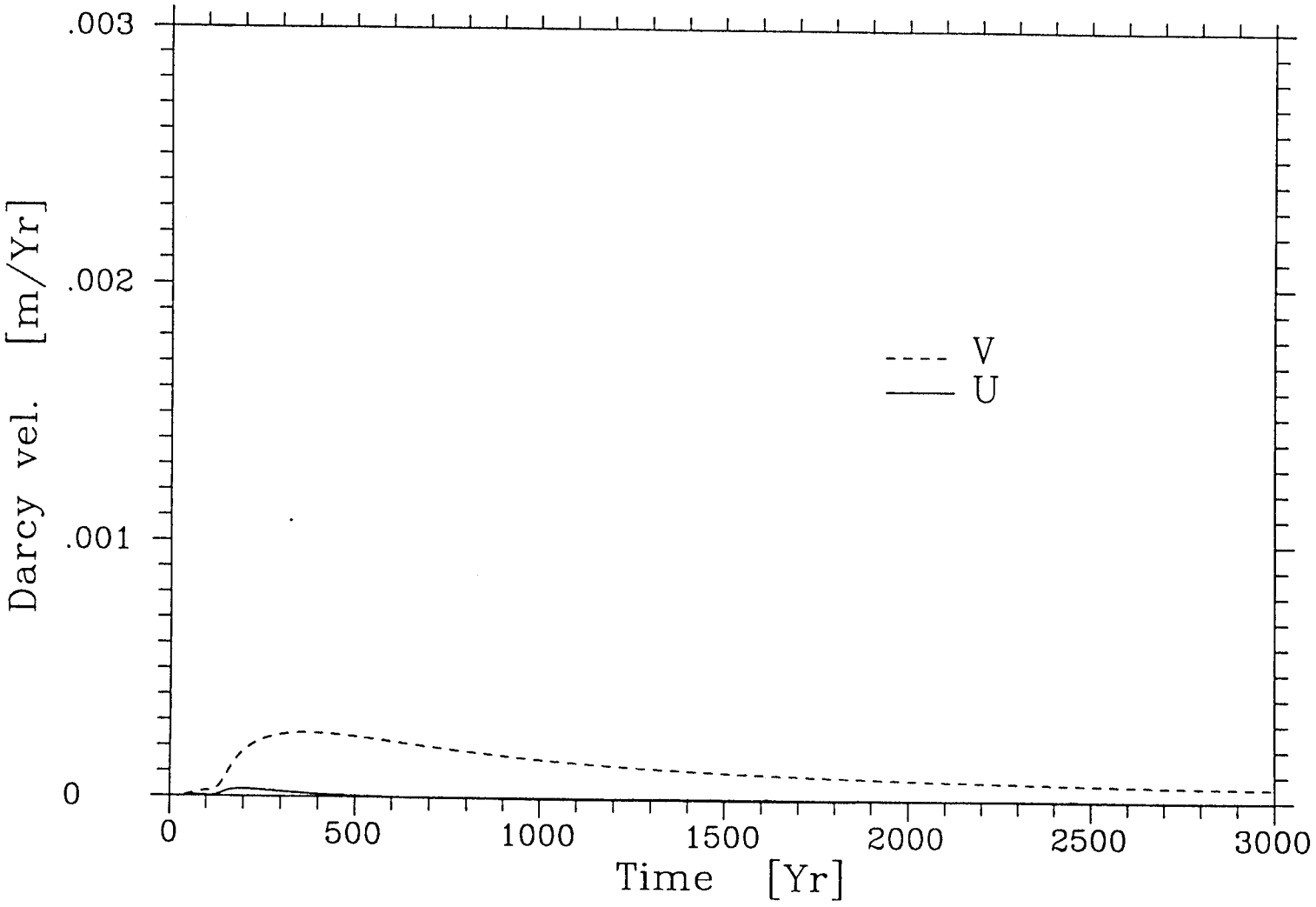

Figure 8: Velocity components at point 2 - case B

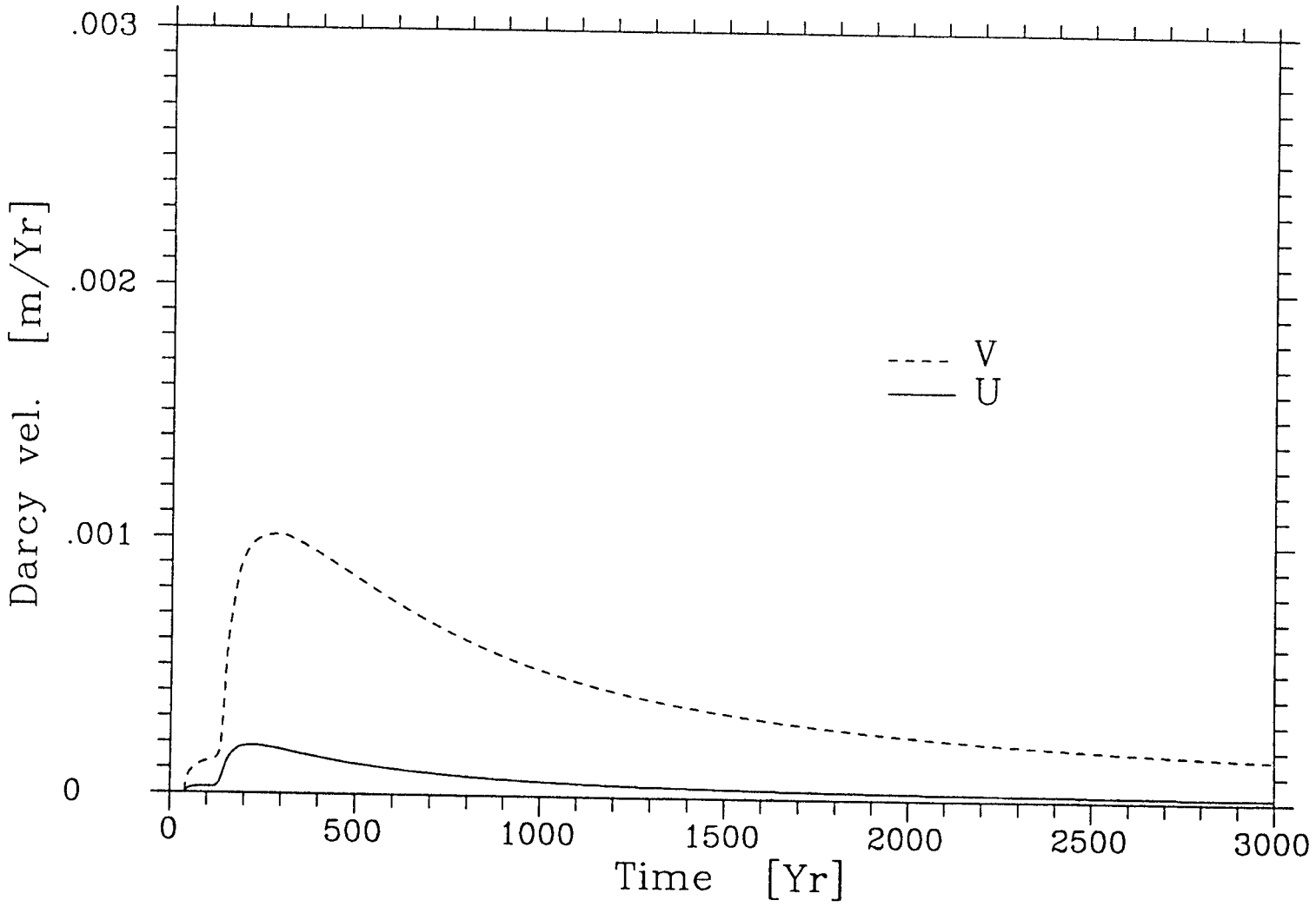

Figure 9: Velocity components at point 2 - case C

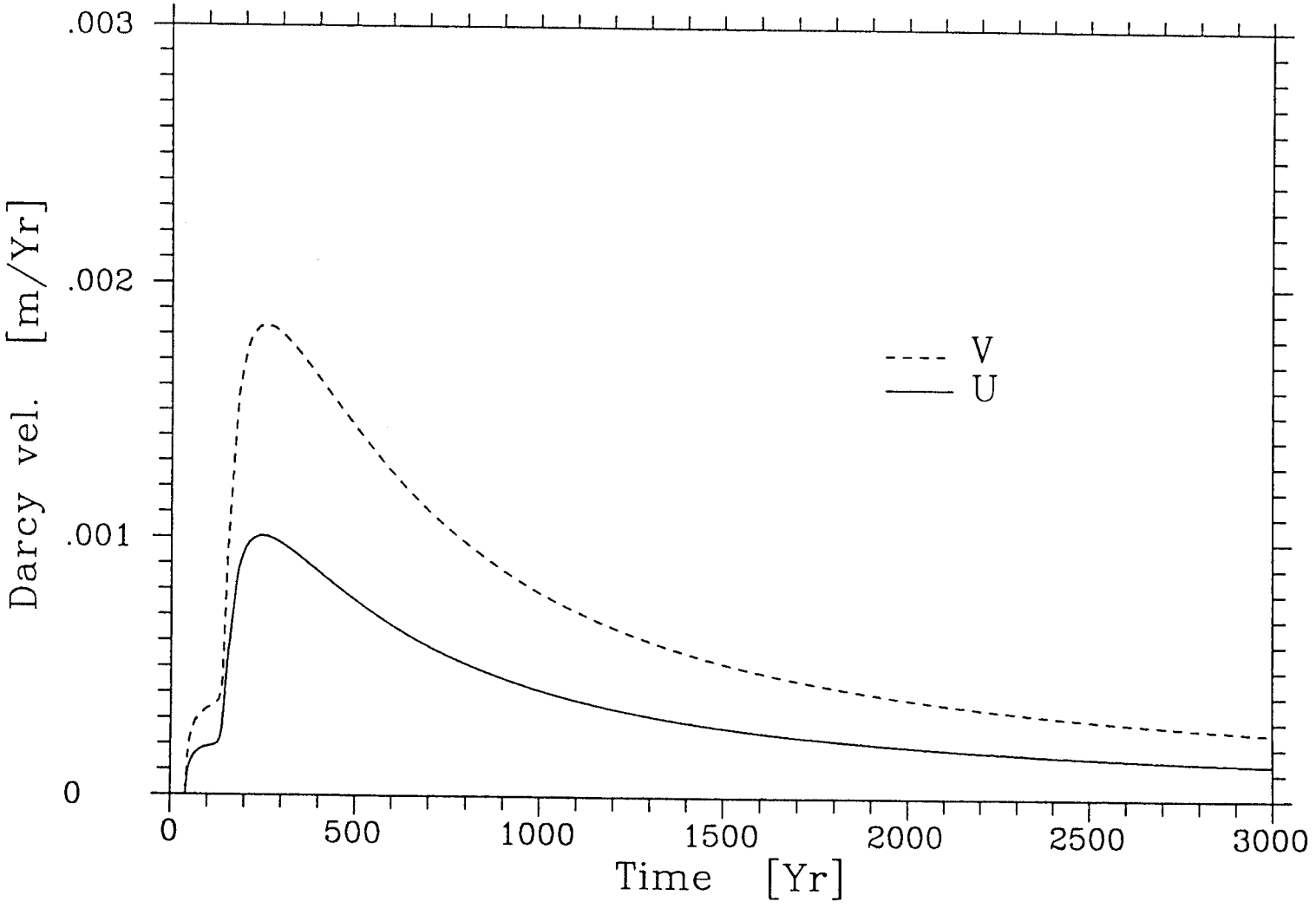

Figure 10: Velocity components at point 3 - case 1

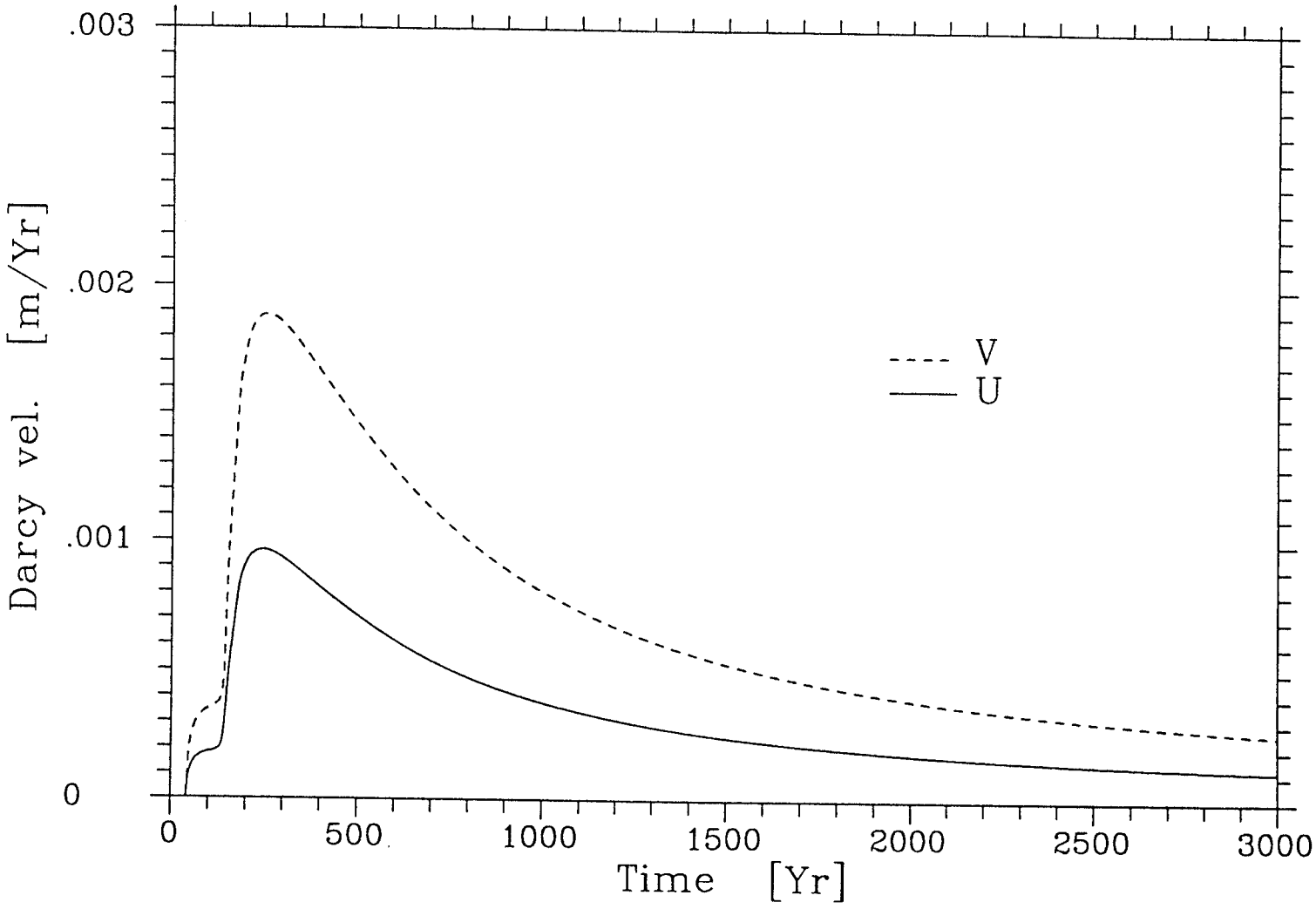

Figure 11: Velocity components at point 3 - case 2

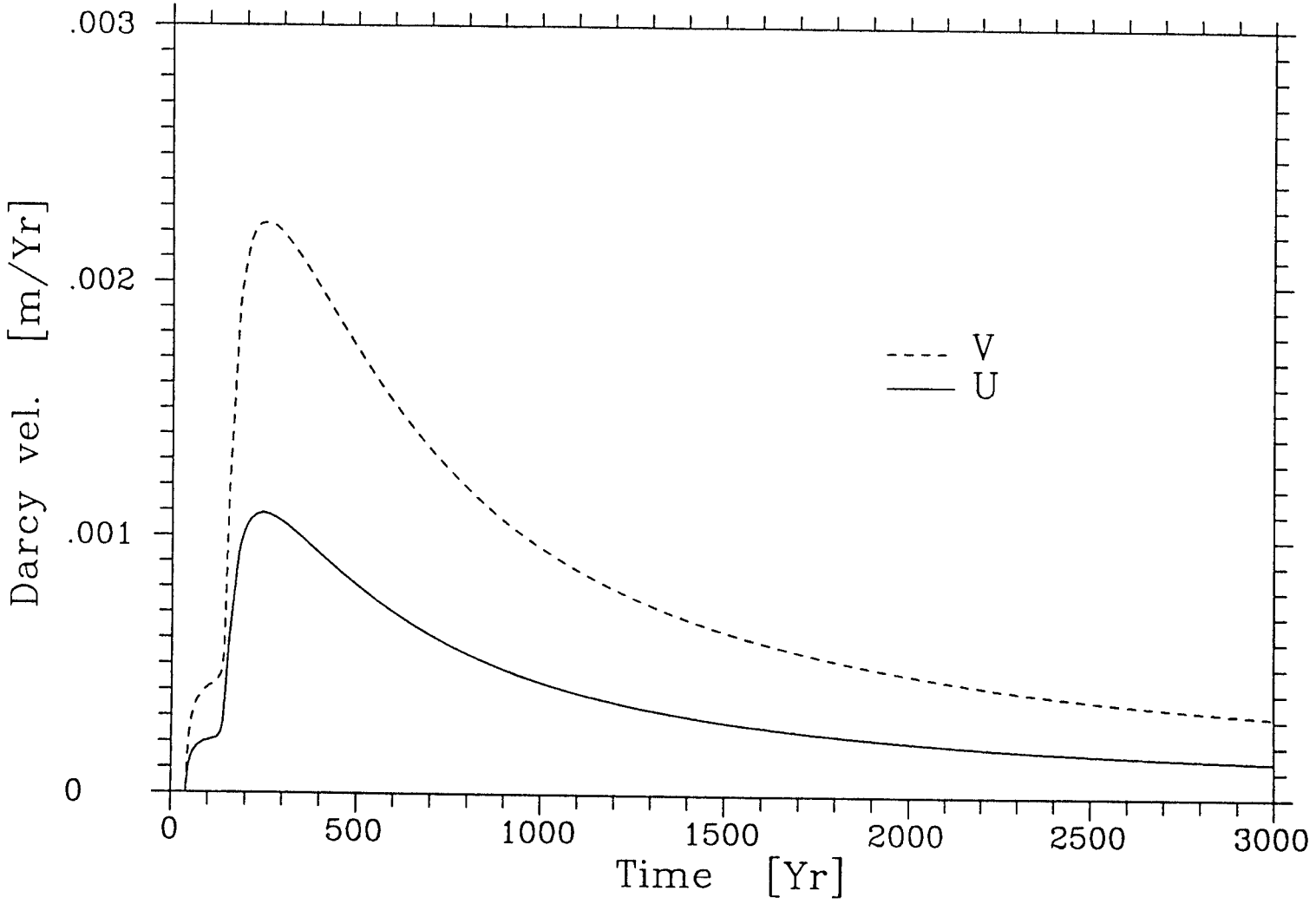

Figure 12: Velocity components at point 3 - case 3

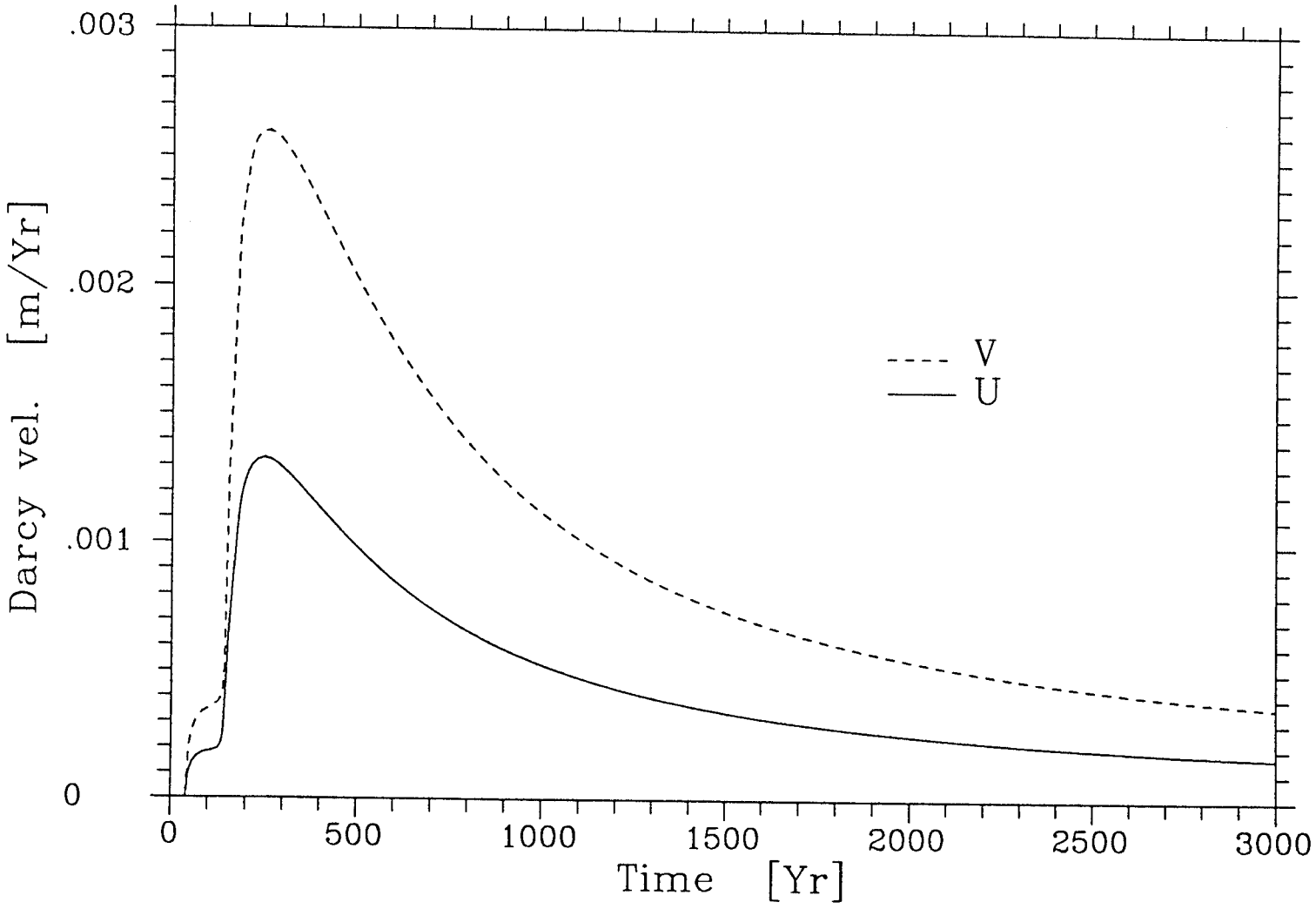

Figure 13: Velocity components at point 3 - case 4

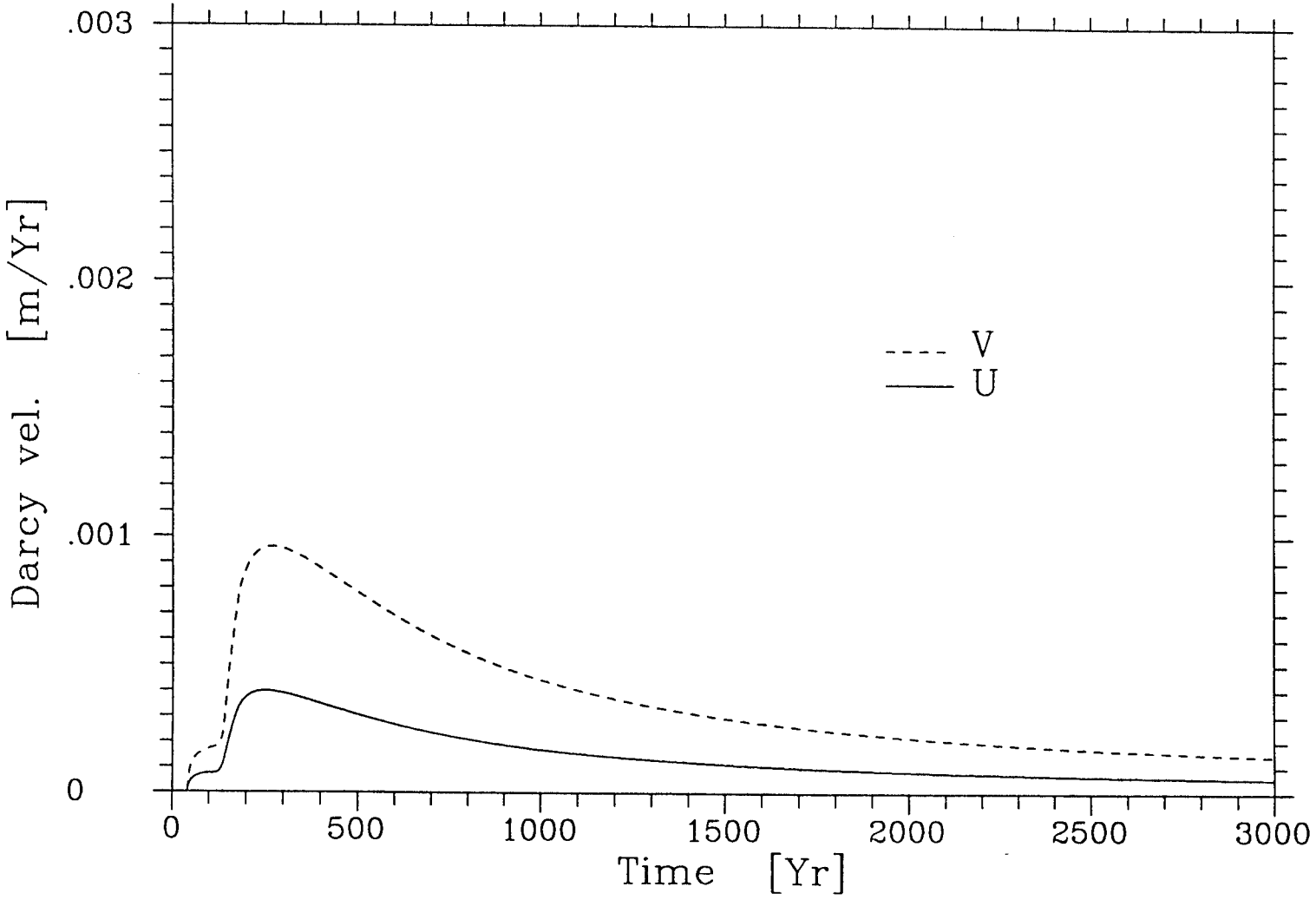

Figure 14: Velocity components at point 3 - case 5

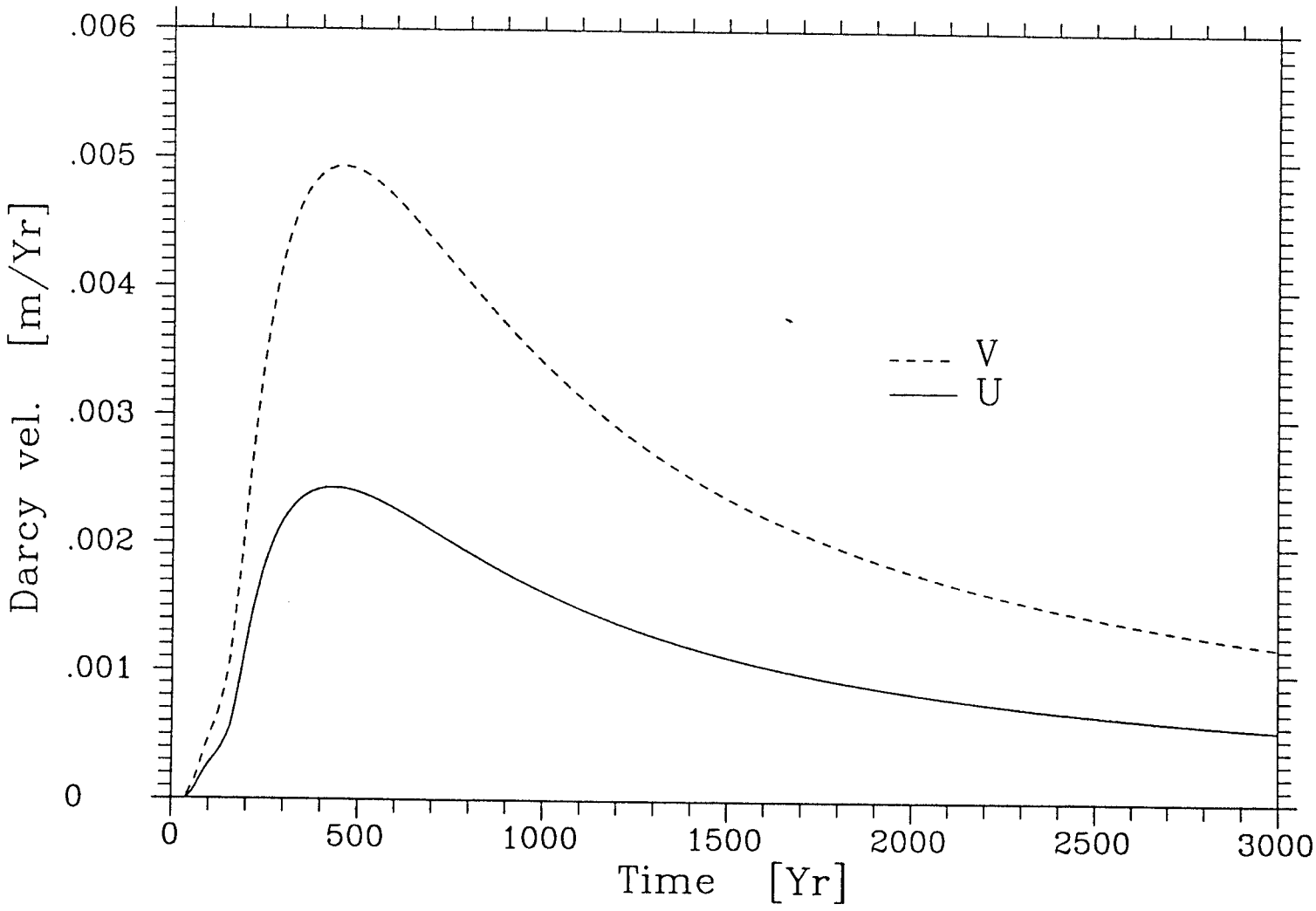

Figure 15: Velocity components at point 3 - case 6

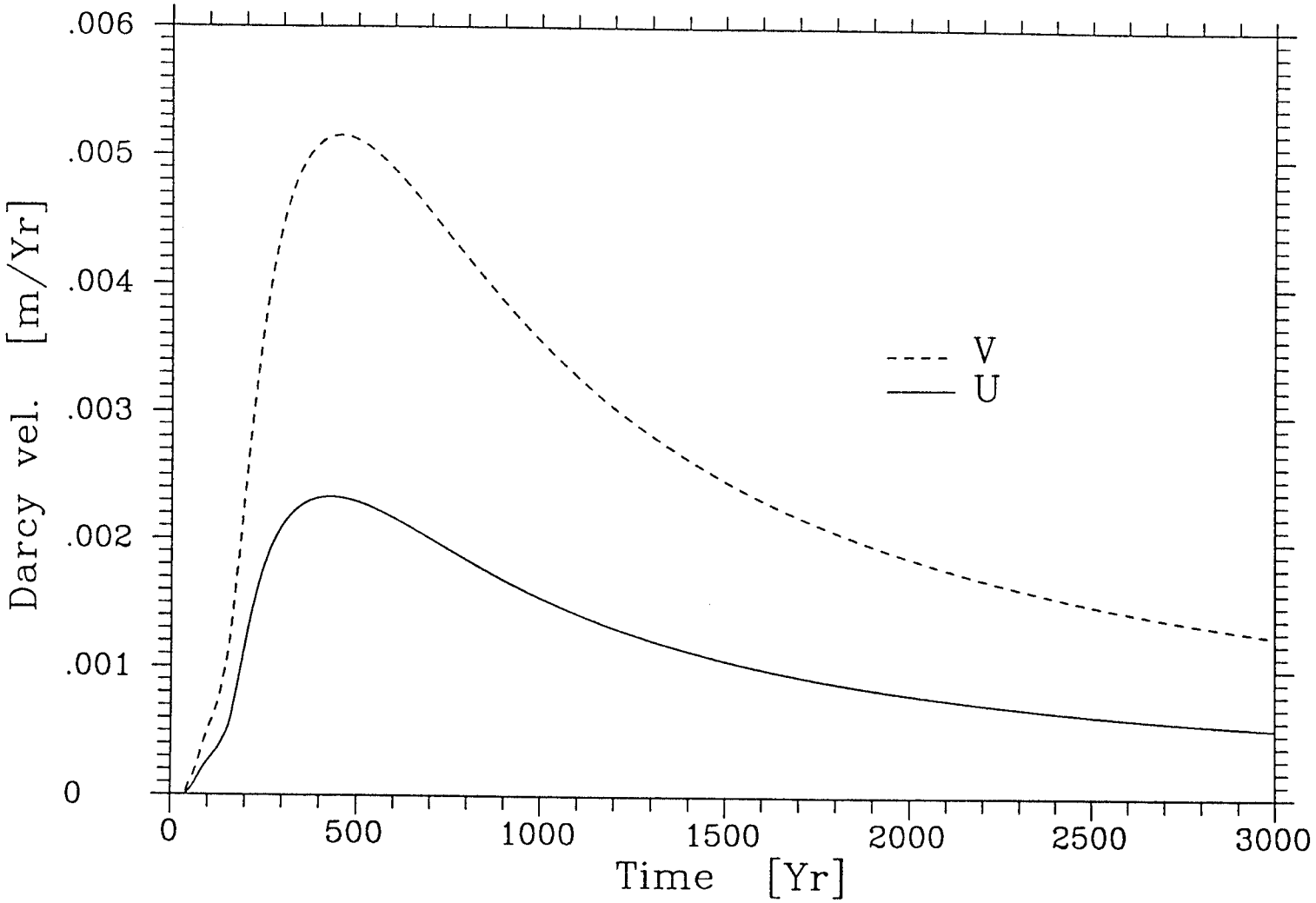

Figure 16: Velocity components at point 3 - case 7

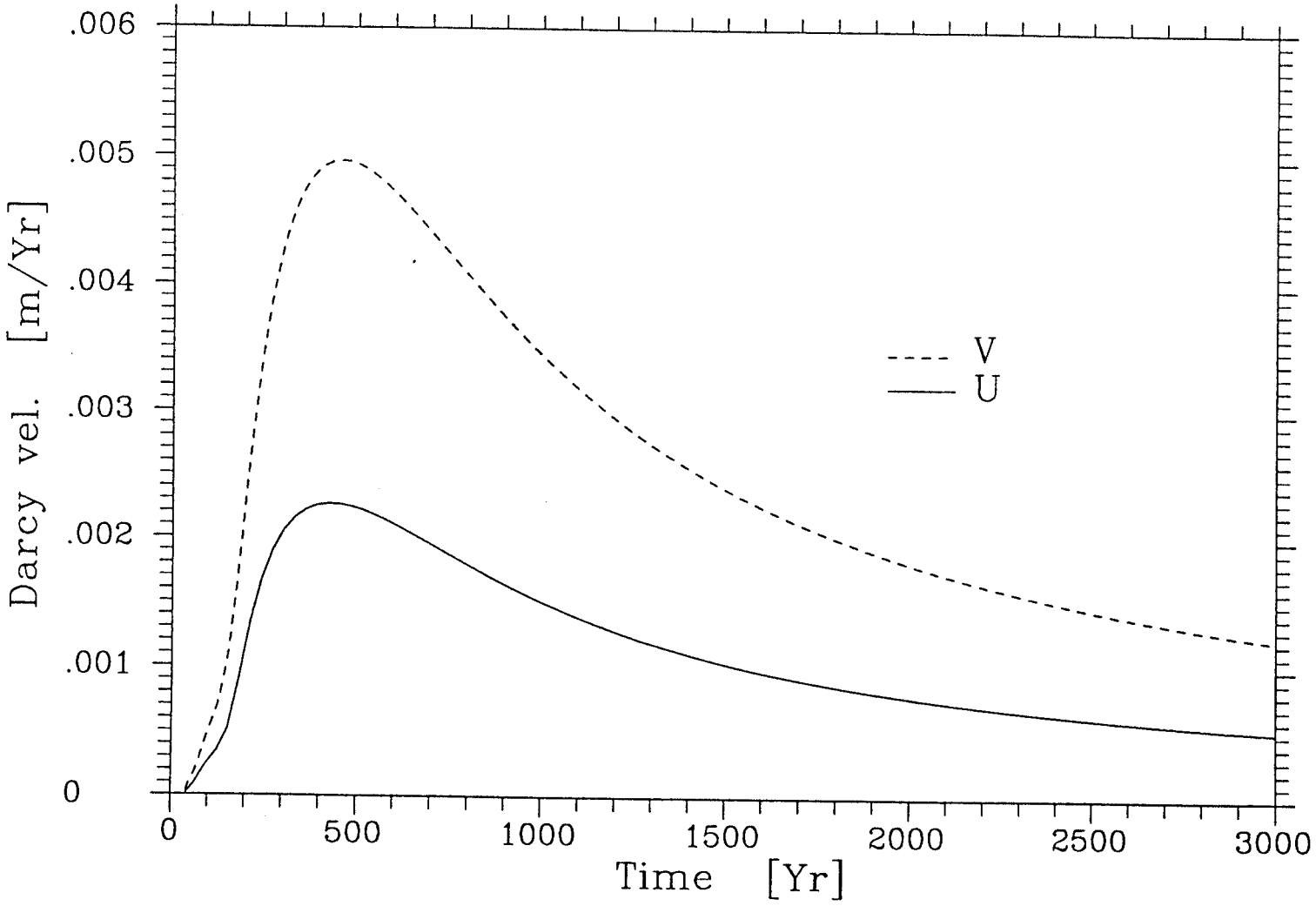

Figure 17: Velocity components at point 3 - case 8

APPENDIX I

APPENDIX I

Basic theory of coupled thermal-hydraulic flows

The algebraic formulation presented in this appendix uses a set of symbols which is explained, together with the relevant units, in the Nomenclature List (Chapter 8 of the main report)

1. Piezometric Head Equation for Flow in a Vertical Plane

A differential equation describing the time varying head distribution in a vertical plane can be derived by considering the continuity criterion for a two-dimensional flow (Bear, [2]). In the Cartesian coordinate system used here, x refers to horizontal and z to vertical distance. Temperature-dependent properties are related to a reference temperature condition, T_r. The total piezometric head or hydraulic potential (h, corresponding to Bear's Φ) is defined by:

$$h = \frac{p}{\rho_r g} + z \qquad \text{(AI.1)}$$

the sum of the pressure head and elevation head.

By using the Boussinesq assumption, whereby density variations affect the vertical component of momentum by imposition of a buoyancy force (= momentum source) but do not affect continuity, together with the Darcy flow relationships, one obtains the general relationship for the Darcy velocity:

$$U_i = -K_{ij} M \left(\frac{\partial h}{\partial x_j} - R \frac{\partial z}{\partial x_j} \right) \qquad \text{(AI.2)}$$

where:

x_i, x_j	are generalised coordinate directions,
z	is the vertical sense and
K_{ij}	is defined at the reference temperature

More specifically, in the vertical (x,z) plane:

$$U = -K_{xx} M \frac{\partial h}{\partial x} \qquad \text{(AI.3.1)}$$

in the horizontal direction and

$$W = -K_{zz} M \left(\frac{\partial h}{\partial z} - R \right) \qquad \text{(AI.3.2)}$$

in the vertical direction.

If these relationships are substituted for the corresponding component velocities in the fluid continuity equation, a new equation for h results:

$$s_p \frac{\partial h}{\partial t} = \frac{\partial}{\partial x}\left(K_{xx} M \frac{\partial h}{\partial x} \right) + \frac{\partial}{\partial z}\left(K_{zz} M \left(\frac{\partial h}{\partial z} - R \right) \right) - s_{th} \frac{\partial T}{\partial t} \qquad \text{(AI.4)}$$

where:

s_p	specific pressure-dependent storage coefficient (Appendix II)
s_{th}	specific temperature-dependent storage coefficient which is treated as a time-varying source term in thermal coupled problems (see also Appendix II)
M (viscosity ratio)	$\frac{\mu_r}{\mu}$
R (density deficit)	$\left(1 - \frac{\rho}{\rho_r} \right)$

The density deficit (R) represents the buoyancy effect in the flow field. It can be calculated as a function of the temperature, R(T), using the expansion coefficient (β) of the fluid, for which data are available:

$$R(T) = 1 - \frac{\rho}{\rho_r} = \int_{T_r}^{T} \frac{\rho(\Theta)}{\rho_r} \beta(\Theta) d\Theta \qquad \text{(AI.5)}$$

In the present case a constant cubical expansion coefficient, a_f, has been employed, resulting in the simplified expression:

$$R(T) = a_f(T - T_r) \tag{AI.6}$$

where:

$$a_f = -\frac{1}{\rho}\frac{\partial \rho}{\partial T} = \frac{1}{v}\frac{\partial v}{\partial T}$$

Under uniform density conditions it is clear that R becomes zero and the buoyancy effect disappears. Equation (AI.4) then describes the flow in a plane of arbitrary orientation. A precisely analogous situation occurs for concentration-dependent fluid density.

Reference 2 has also provided expressions for temperature and pressure dependence of viscosity and thermal conductivity of water.

2. Thermal Energy Transport in a Porous Medium

The heat transport in a fluid-saturated porous medium takes place both in the liquid and in the solid components: in the solid by conduction only, in the liquid both by conduction and by convection.

The transport equations are:

$$\frac{\partial}{\partial t}((1-n)\rho_s C_s T_s) = \frac{\partial}{\partial x}\left((1-n)k_s\frac{\partial T_s}{\partial x}\right) + \frac{\partial}{\partial z}\left((1-n)k_s\frac{\partial T_s}{\partial z}\right) + (1-n)S^T_{s,t} \tag{AI.7}$$

for the solid and

$$\frac{\partial}{\partial t}(n\rho_l C_l T_l) + \frac{\partial}{\partial x}(n\rho_l u C_l T_l) + \frac{\partial}{\partial z}(n\rho_l w C_l T_l) = \frac{\partial}{\partial x}\left(nk_l\frac{\partial T_l}{\partial x}\right) + \frac{\partial}{\partial z}\left(nk_l\frac{\partial T_l}{\partial z}\right) + nS^T_l \tag{AI.8}$$

for the fluid, where:

S^T	is a general, time varying source term [W m^{-3}]
s, l	are suffices referring to solid and liquid respectively
u, w	are hydraulic (pore water) flow velocities

The source terms contain the heat flux between solid and liquid in addition to possible heat sources. At slow groundwater flows thermal equilibrium between solid and fluid can be assumed with good justification. Then, at any location, the temperatures of the solid and liquid will always be equal ($T_s = T_l$). In this case, the heat transport problem is simplified drastically, the process being described by one equation only:

$$\frac{\partial}{\partial t}(\overline{\rho C}T) + \frac{\partial}{\partial x}(n\rho_l u C_l T) + \frac{\partial}{\partial z}(n\rho_l w C_l T) = \frac{\partial}{\partial x}\left(\overline{k}_x \frac{\partial T}{\partial x}\right) + \frac{\partial}{\partial z}\left(\overline{k}_z \frac{\partial T}{\partial z}\right) + S^T \qquad \text{(AI.9)}$$

where the source terms represent heat sources in the calculation domain and:

$$\overline{k}_{x_i} = (k_s^{(1-n)} \cdot k_l^n)_{x_i}$$

$$\overline{\rho C} = (1-n)\rho_s C_s + n\rho_l C_l$$

It should be noted that the above expression for effective thermal conductivity (see Ref. 3) does not include the effect of hydrodynamic dispersion upon the value of the effective fluid conductivity. This effect has been ignored in the current version of TROUGH-2DP, since its influence at low flow speed in low porosity materials, where material conductivity tends to exceed fluid conductivity, is expected to be small.

3. Method of Solution

Equation (AI.4) and (AI.9) are the two equations which are solved in coupled fashion in the present model. The former, developed from the fluid continuity relationship represents diffusion of potential, the latter represents combined diffusion and advection of thermal energy.

The computer code TROUGH-2DP uses the implicit formulation of the finite difference versions of (AI.4) and (AI.9). That is to say coefficients where solution-dependent, are calculated iteratively in terms of the unknown field values at the end of each timestep.

An iterative solution to the field matrix equation which is set up from the resulting algebraic equations for each nodal point in the domain is made by Gaussian Elimination.

When coupled processes are to be studied, as in the present case, the corresponding equations are solved iteratively and alternately until a converged solution for the current timestep is reached. This is necessary since the temperature distribution determines the buoyancy sources in the hydraulic potential equation and the resulting fluid velocities determine the advective heat transport terms in the thermal energy equation.

APPENDIX II

APPENDIX II

Changes in the Mass of Fluid Stored in the Pores of a Saturated, Porous Medium Under Conditions of Varying Pressure and Temperature

This process can in some circumstances strongly affect transient flow processes. The fact that the temperature also varies in the present case leads us to derive the relationships leading to the time-dependent term in the equation of mass conservation. This term defines the rate of change of mass of pore fluid per unit volume of bulk material:

$$\frac{dm}{dt} = \frac{d}{dt}(n\rho_f) = \frac{d}{dt}(v_f\rho_f) \qquad \text{(AII.1)}$$

where sufix f refers to the fluid and:

v_f volume fraction of fluid (= porosity n)

ρ_f fluid density

If the suffix s refers to the solid portion we can also define:

v_s as the volume fraction of the solid (= (1-n))

And we have: $v_s + v_f = 1$ (AII.2)

We must now rewrite (AII.1) in terms of partial differentials:

$$\begin{aligned}\frac{dm}{dt} &= \frac{d}{dt}(v_f\rho_f) \\ &= v_{f0}\frac{\partial}{\partial t}\rho_f\Big|_{v_f} + \rho_{f0}\frac{\partial}{\partial t}v_f\Big|_{\rho_f} \qquad \text{(AII.3)} \\ &= v_{f0}\left\{\frac{\partial\rho_f}{\partial S_m}\frac{\partial S_m}{\partial t}+\frac{\partial\rho_f}{\partial p}\frac{\partial p}{\partial t}+\frac{\partial\rho_f}{\partial T}\frac{\partial T}{\partial t}\right\}\Big|_{v_f} + \rho_{f0}\left\{\frac{\partial v_f}{\partial S_m}\frac{\partial S_m}{\partial t}+\frac{\partial v_f}{\partial p}\frac{\partial p}{\partial t}+\frac{\partial v_f}{\partial T}\frac{\partial T}{\partial t}\right\}\Big|_{\rho_f}\end{aligned}$$

using the most general form, including dependences upon mean stress level, pore pressure and temperature.

We can say that:

$$\frac{\partial \rho_f}{\partial S_m} = 0 \qquad \frac{\partial \rho_f}{\partial p} = \frac{\rho_{f0}}{K_f} \qquad \frac{\partial \rho_f}{\partial T} = \rho_{f0} a_f$$

and noting that changes in porosity are determined by changes in the volume fraction of the solid. The fluid density does not depend on mean stess level in the solid.

We note from (AII.2) that:

$$\partial v_f = -\partial v_s$$

so that:

$$\frac{\partial v_f}{\partial S_m} = \frac{\alpha}{K_b} \qquad \frac{\partial v_f}{\partial p} = \left(\frac{\alpha}{K_b} - \frac{v_{f0}}{K_s} \right) \qquad \frac{\partial v_f}{\partial T} = (a_b - (1 - v_{f0}) a_s)$$

If in the second term of (AII.3) the dependence on mean stress may be neglected, the relationship can be rewritten as follows:

$$\begin{aligned} \frac{dm}{dt} &= \left\{ v_{f0} \frac{\partial \rho_f}{\partial p} + \rho_{f0} \frac{\partial v_f}{\partial p} \right\} \frac{\partial p}{\partial t} + \left\{ v_{f0} \frac{\partial \rho_f}{\partial T} + \rho_{f0} \frac{\partial v_f}{\partial T} \right\} \frac{\partial T}{\partial t} \\ &= \left\{ \rho_{f0} v_{f0} \left(\frac{1}{K_f} - \frac{1}{K_s} \right) + \frac{\alpha \rho_{f0}}{K_b} \right\} \frac{\partial p}{\partial t} + \{ \rho_{f0} v_{f0} (a_f + a_s) + \rho_{f0} (a_b - a_s) \} \frac{\partial T}{\partial t} \end{aligned} \qquad \text{(AII.4)}$$

Using the relationship:

$$p = \rho_r g h$$

it becomes possible to rewrite (AII.4) in terms of hydraulic head h, rather than pore pressure p. This enables the storage coefficients for equation (AI.4) in Appendix I to be defined:

$$\frac{d(n\rho_f)}{dt} = S_p \frac{\partial h}{\partial t} + S_{th} \frac{\partial T}{\partial t}$$

Thus for the case where stress changes are neglected:

$$S_p = \rho_r \left\{ \rho_{f0} v_{f0} \left(\frac{1}{K_f} - \frac{1}{K_s} \right) + \frac{\alpha \rho_{f0}}{K_b} \right\}$$

$$S_{th} = \{ \rho_{f0} v_{f0} (a_f + a_s) + \rho_{f0} (a_b - a_s) \}$$

List of SKB reports

Annual Reports

1977–78
TR 121
KBS Technical Reports 1 – 120.
Summaries. Stockholm, May 1979.

1979
TR 79–28
The KBS Annual Report 1979.
KBS Technical Reports 79-01 – 79-27.
Summaries. Stockholm, March 1980.

1980
TR 80–26
The KBS Annual Report 1980.
KBS Technical Reports 80-01 – 80-25.
Summaries. Stockholm, March 1981.

1981
TR 81–17
The KBS Annual Report 1981.
KBS Technical Reports 81-01 – 81-16.
Summaries. Stockholm, April 1982.

1982
TR 82–28
The KBS Annual Report 1982.
KBS Technical Reports 82-01 – 82-27.
Summaries. Stockholm, July 1983.

1983
TR 83–77
The KBS Annual Report 1983.
KBS Technical Reports 83-01 – 83-76
Summaries. Stockholm, June 1984.

1984
TR 85–01
Annual Research and Development Report 1984
Including Summaries of Technical Reports Issued during 1984. (Technical Reports 84-01–84-19)
Stockholm June 1985.

1985
TR 85-20
Annual Research and Development Report 1985
Including Summaries of Technical Reports Issued during 1985. (Technical Reports 85-01-85-19)
Stockholm May 1986.

1986
TR 86-31
SKB Annual Report 1986
Including Summaries of Technical Reports Issued during 1986
Stockholm, May 1987

1987
TR 87-33
SKB Annual Report 1987
Including Summaries of Technical Reports Issued during 1987
Stockholm, May 1988

1988
TR 88-32
SKB Annual Report 1988
Including Summaries of Technical Reports Issued during 1988
Stockholm, May 1989

Technical Reports

1989

TR 89-01
Near-distance seismological monitoring of the Lansjärv neotectonic fault region Part II: 1988
Rutger Wahlström, Sven-Olof Linder, Conny Holmqvist, Hans-Edy Mårtensson
Seismological Department, Uppsala University, Uppsala
January 1989

TR 89-02
Description of background data in SKB database GEOTAB
Ebbe Eriksson, Stefan Sehlstedt
SGAB, Luleå
February 1989

TR 89-03
Characterization of the morphology, basement rock and tectonics in Sweden
Kennert Röshoff
August 1988

TR 89-04
SKB WP-Cave Project
Radionuclide release from the near-field in a WP-Cave repository
Maria Lindgren, Kristina Skagius
Kemakta Consultants Co, Stockholm
April 1989

TR 89-05
SKB WP-Cave Project
Transport of escaping radionuclides from the WP-Cave repository to the biosphere
Luis Moreno, Sue Arve, Ivars Neretnieks
Royal Institute of Technology, Stockholm
April 1989

TR 89-06

SKB WP-Cave Project

Individual radiation doses from nuclides contained in a WP-Cave repository for spent fuel

Sture Nordlinder, Ulla Bergström
Studsvik Nuclear, Studsvik

April 1989

TR 89-07

SKB WP-Cave Project

Some Notes on Technical Issues

Part 1: Temperature distribution in WP-Cave: when shafts are filled with sand/water mixtures
Stefan Björklund, Lennart Josefson
Division of Solid Mechanics, Chalmers University of Technology, Gothenburg, Sweden

Part 2: Gas and water transport from WP-Cave repository Luis Moreno, Ivars Neretnieks
Department of Chemical Engineering, Royal Institute of Technology, Stockholm, Sweden

Part 3: Transport of escaping nuclides from the WP-Cave repository to the biosphere. Influence of the hydraulic cage
Luis Moreno, Ivars Neretnieks
Department of Chemical Engineering, Royal Institute of Technology, Stockholm, Sweden

August 1989